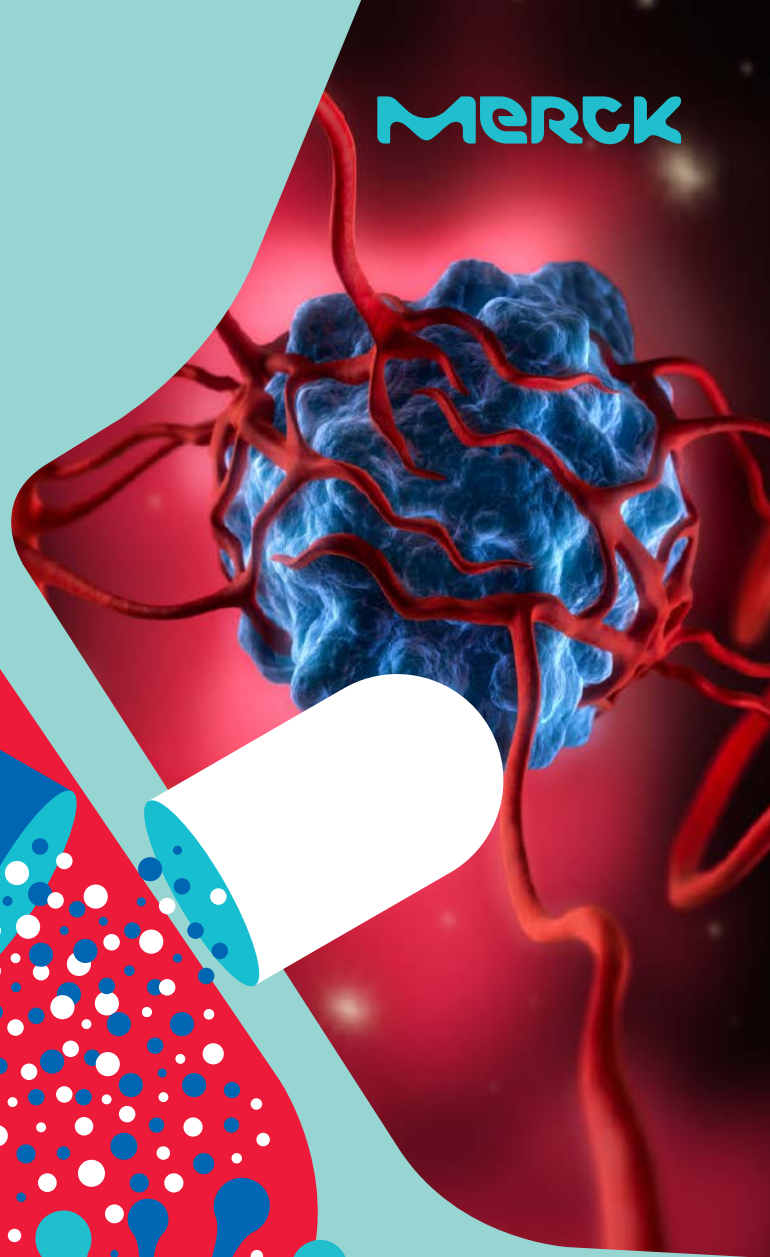


Material Matters™

VOLUME 15 • NUMBER 3



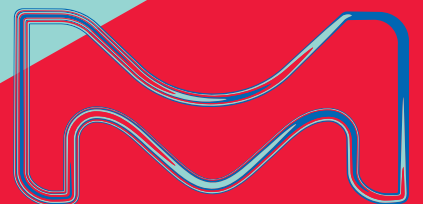
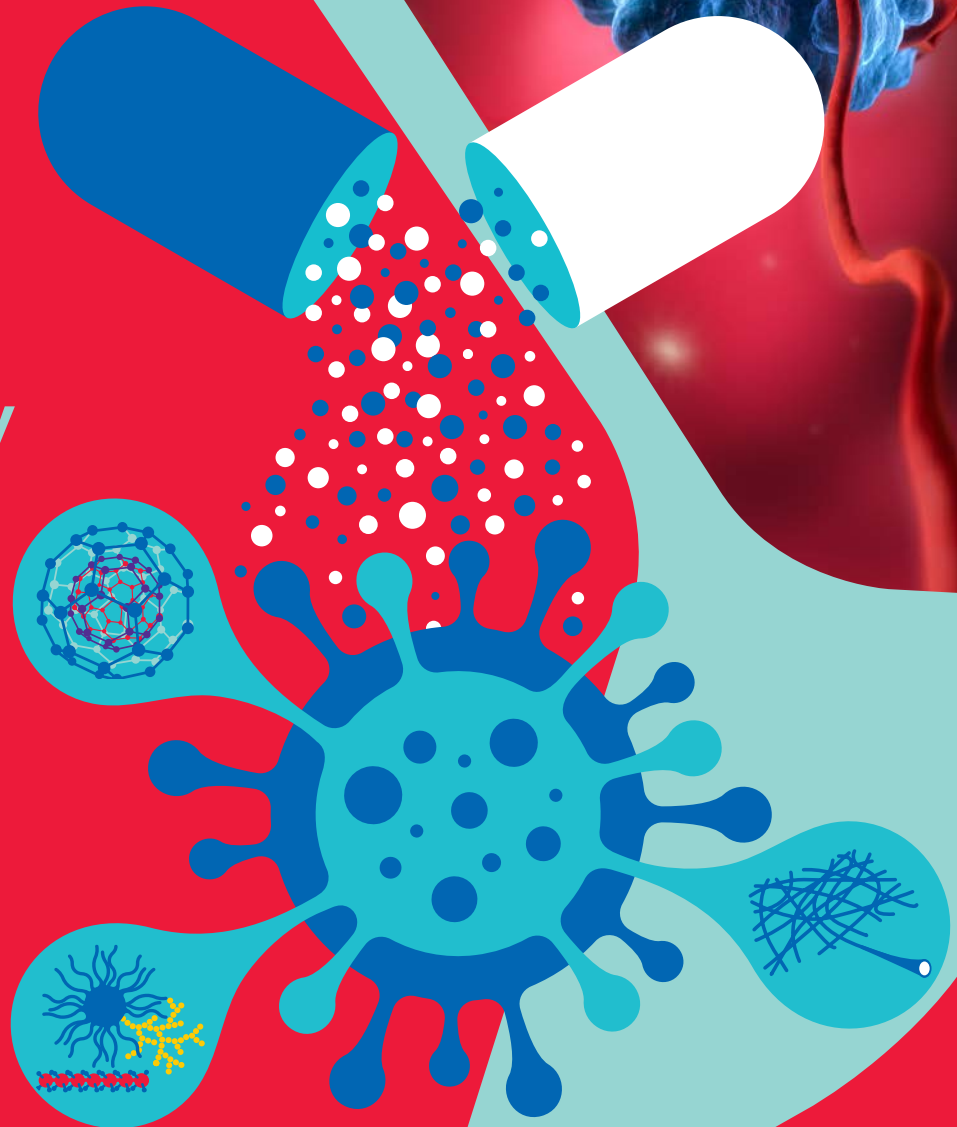
Advanced Tools for Drug Delivery Research

Flash NanoPrecipitation (FNP) – Principles and Applications in Medical Imaging and Drug Delivery

Recent Progress on Nonviral Delivery Carriers for CRISPR/Cas9 Systems

Smart Nanofiber Meshes as a Local Drug Delivery Platform

The Potential of Dendritic Polyester Scaffolds as Biocompatible Drug Delivery Agents



Introduction



Hanying Luo, Ph.D.
Global Product
Manager –
Biomedical Materials

Welcome to the third issue of *Material Matters*™ for 2020, presenting innovative technology platforms that enable drug delivery and medical imaging applications. This issue highlights flash nanoprecipitation, an innovative approach to producing well-defined nanoparticles loaded with drug or contrast agents for biomedical applications. Also, it features the potentials of nanocarriers to tackle challenges in novel therapeutics delivery, such as CRISPR.

Nanoparticles have demonstrated great potential in many biomedical applications, including drug delivery, bioimaging, and diagnostics. In the first article, **Professor Robert K. Prud'homme (Princeton University, USA)** introduces flash nanoprecipitation (FNP) for nanoparticle fabrication. FNP is a scalable, rapid mixing process for nanoparticle formulations. FNP allows the production of a wide variety of molecules, from hydrophobic small molecules to oligonucleotides, peptides, and proteins, opening the door for more innovation in nanoparticle-based therapies and diagnostics.

The CRISPR/Cas9 system has recently emerged as a highly specific, efficient, and versatile gene editing technology that can be utilized to build disease models and correct diseased genes. Safe and effective delivery vectors for the CRISPR/Cas9 system are in critical need to enable clinical development and future applications of CRISPR/Cas9 systems. In the second article, **Professor Yang Liu (Nankai University, China)** summarizes recent progress in nonviral nanoparticle approaches for CRISPR/Cas9 delivery.

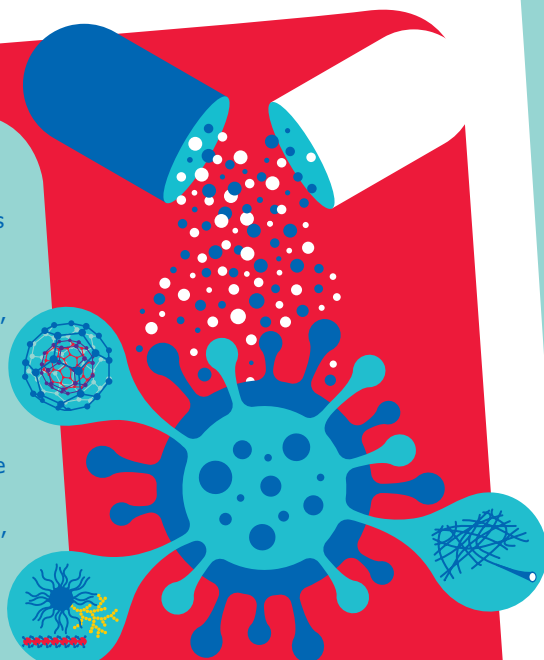
In the third article, **Professor Mitsuhiro Ebara (National Institute for Materials Science (NIMS), Japan)** provides insights on several types of smart nanofiber mesh systems that have been explored for different drug delivery purposes. These biodegradable nanofibers provide targeted therapeutic treatment with improved drug efficacy.

Dendrimers, dendrons and linear dendritic hybrids comprise a family of synthetic macromolecules containing a large number of branches, and thus a multitude of peripheral groups. In the fourth article, **Professor Michael Malkoch (KTH Royal Institute of Technology, Sweden)** provides an overview of the unique properties of dendritic molecules and their application in biomedical fields. He highlights bis-MPA dendritic scaffolds as a promising biodegradable and biocompatible platform for drug delivery applications.

Each article in this issue is accompanied by a list of related products available from the Merck portfolio. Please visit [SigmaAldrich.com/matsci](https://www.sigmaaldrich.com/matsci) for additional product offerings and information. As always, please 'bother' us with new product suggestions and your feedback at [SigmaAldrich.com/technicalservice](https://www.sigmaaldrich.com/technicalservice).

About the Cover

Innovative drug delivery platforms have been developed as effective approaches to transform the drug release profiles, pharmacokinetics, and pharmacodynamics parameters and to improve drug efficacy and safety. They also have the potential to enable novel therapeutics, such as CRISPR. The cover art for this issue highlights a few novel drug delivery systems, including polymeric and inorganic nanoparticles, dendrimers, and nano meshes for delivering therapeutics.



Merck KGaA
Frankfurter Strasse 250
64293 Darmstadt, Germany
Phone +49 6151 72 0

To Place Orders / Customer Service

Contact your local office or visit
[SigmaAldrich.com/order](https://www.sigmaaldrich.com/order)

Technical Service

Contact your local office or visit
[SigmaAldrich.com/techinfo](https://www.sigmaaldrich.com/techinfo)

General Correspondence

Contact your local office or visit
[SigmaAldrich.com/techinfo](https://www.sigmaaldrich.com/techinfo)

Subscriptions

Request your FREE subscription to *Material Matters*™ at [SigmaAldrich.com/mm](https://www.sigmaaldrich.com/mm)

The entire *Material Matters*™ archive is available at [SigmaAldrich.com/mm](https://www.sigmaaldrich.com/mm)

Material Matters™ (ISSN 1933-9631) is a publication of Merck KGaA.

Copyright © 2020 Merck KGaA, Darmstadt, Germany and/or its affiliates. All rights reserved. Merck, the vibrant M, SigmaAldrich and Material Matters are trademarks of Merck KGaA, Darmstadt, Germany or its affiliates. All other trademarks are the property of their respective owners. Detailed information on trademarks is available via publicly accessible resources. More information on our branded products and services on [MerckMillipore.com](https://www.MerckMillipore.com)

Your Material Matters



Bryce P. Nelson, Ph.D.
Materials Science Initiative Lead

Professor Shlomo Magdassi at the Hebrew University of Jerusalem recommended the addition of water-soluble TPO based nanoparticle photoinitiators (**Cat. No. 906808** and **906816**) to our catalog to enable aqueous photopolymerizations.

Water-soluble photoinitiators with high absorbance in the UV-visible range are needed to enable the rapid 3D printing of hydrogels for drug delivery and tissue engineering applications.¹⁻⁴ Recently, water-dispersible nanoparticles of 2,4,6-trimethylbenzoyl-diphenylphosphine oxide (TPO) have been developed, and they possess much larger extinction coefficient compared with the best and most used commercially available water-soluble photoinitiator.¹ TPO nanoparticles absorb significantly in the range from 385 to 420 nm, making them suitable for use in commercially available, low-cost, light-emitting diode-based 3D printers using digital light processing. The polymerization rate at this range is very fast and enables 3D printing that is otherwise impossible to perform without adding solvents.¹ Such water-dispersible photoinitiator nanoparticles expand the many opportunities for 3D printing of structures prepared in aqueous solutions while bringing environmental advantages by using low-energy curing systems and avoiding the need for solvents.

References

- (1) Pawar, A. A.; Saada, G.; Cooperstein, I.; Larush, L.; Jackman, J. A.; Tabaei, S. R.; Cho, N.; Magdassi, S. *Sci. Adv.* **2016**, *2* (4), e1501381.
- (2) Larush, L.; Kaner, I.; Fluksman, A.; Tamsut, A.; Pawar, A. A.; Lesnovski, P.; Benny, O.; Magdassi, S. *J. 3D Print. Med.* **2017**, *1* (4), 219-229.
- (3) Fairbanks, B. D.; Schwartz, M. P.; Bowman, C. N.; Anseth, K. S. *Biomaterials* **2009**, *30*, 6702-6707.
- (4) Williams, C. G.; Malik, A. N.; Kim, T. K.; Manson, P. N.; Elisseeff, J. H. *Biomaterials* **2005**, *26*, 1211-1218.

Name	Cat. No.
Water-soluble TPO based nanoparticle photoinitiator	906816-1G 906816-5G 906808-1G 906808-5G

Table of Contents

Articles

Flash NanoPrecipitation (FNP) — Principles and Applications in Medical Imaging and Drug Delivery	95
Recent Progress on Nonviral Delivery Carriers for CRISPR/Cas9 Systems	104
Smart Nanofiber Meshes as a Local Drug Delivery Platform	113
The Potential of Dendritic Polyester Scaffolds as Biocompatible Drug Delivery Agents	119

Featured Products

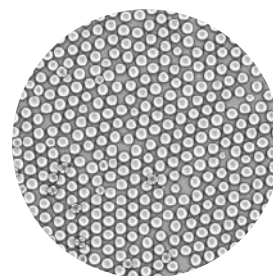
A list of NanoFabTX™ Formulation Kits A list of ready-to-use microfluidics kits	100
Biodegradable Poly(lactide-co-glycolide) A selection of poly(lactide-co-glycolide) materials	100
Biodegradable Diblock Copolymers A selection of poly(ethylene glycol) diblock copolymers	101
Functionalized Biodegradable Diblock Copolymers A selection of poly(ethylene glycol) diblock copolymers	101
Polyethylenimine (PEI) Selections of linear, branched, and modified PEIs	109
Functionalized Poly(ethylene glycol) (PEG) A selection of PEGs	110
Gold Nanoparticles A selection of gold nanoparticles for drug delivery	111
Graphene Oxide A list of GO materials for drug delivery	111
Biodegradable Poly(caprolactone) A selection of poly(caprolactone)	117
Responsive Polymers Selections of poly(N-isopropylacrylamide) polymers and copolymers	117
Magnetic Nanoparticles A list of FeO magnetic nanoparticles	118
Bis-MPA Dendritic Scaffolds A selection of dendrimers and dendrons for drug delivery	123

Formulation Made Easier

NanoFabTx™ Formulation Kits

Formulate faster with our ready-to-use NanoFabTx™ formulation kits. NanoFabTx™ kits provide more reproducible synthesis from nano- to micro-sized particles, using both standard nanoprecipitation and microfluidic techniques. NanoFabTx™ kits facilitate early-stage drug nanoformulation screening with optimized protocols and a curated selection of polymer-based materials for drug encapsulation.

NanoFabTx™ reagent kits can be used with easy-to-use nanoprecipitation methods or can also leverage the power of microfluidics when combined with NanoFabTx™ microfluidic device kits. Together, these kits enable simplified and rapid synthesis of monodispersed particles with minimal batch-to-batch variability. Device kits include pre-assembled microfluidic glass chips, tubing, and accessories, that are ready for connection with a fluid pump system such as the Dolomite Nanoparticle Generation System.



Key Features:

- Step-by-step protocols developed and tested by our formulation scientists
- Flexible synthesis tool to create uniform and reproducible nanoparticles
- Choose from standard glassware-based nanoprecipitation or microfluidic-based protocols
- Optimized to make nanoparticles 100–200 nm or microparticles 1–30 μm by nanoprecipitation or microfluidics with low polydispersity
- Based on non-toxic, biodegradable polymers
- Material screening kits available

Applications:

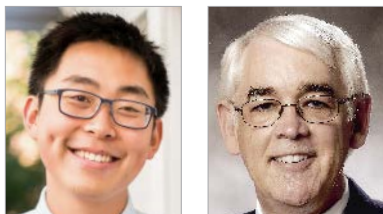
- Screening and selection of optimal formulation
- Selection of optimal size
- Optimization of drug encapsulation and loading efficiency
- Screening the optimal nano- and micro-formulation for enhancing drug bioavailability

For a complete list of NanoFabTx™ formulation kits, visit

[SigmaAldrich.com/nanofabtx](https://www.sigmaaldrich.com/nanofabtx)



Flash NanoPrecipitation (FNP) — Principles and Applications in Medical Imaging and Drug Delivery



Leon Z. Wang, Robert K. Prud'homme*

Department of Chemical and Biological Engineering, Princeton University, Princeton, New Jersey 08544, United States.
*Email: prudhomm@Princeton.EDU

Introduction

The principle of Flash NanoPrecipitation (FNP) was first described in 2003 by Johnson and Prud'homme as a novel method to generate highly loaded nanoparticles through a rapid mixing and precipitation process.¹ FNP technology has since grown to impact a variety of fields ranging from drug encapsulation to pesticide delivery. FNP is a scalable mixing process that takes advantage of the different timescales of nucleation, aggregation, and stabilization. In the most basic form, a highly hydrophobic molecule and an amphiphilic polymer are dissolved in a water-miscible organic solvent. This organic stream is then mixed rapidly with an aqueous anti-solvent stream using specially designed turbulent mixing chambers. During this mixing, competing kinetic processes are ongoing: (1) Nucleation and aggregation of the hydrophobic active, (2) Adsorption of the steric stabilizing polymer on the aggregate, which ultimately arrests further growth. The ratio of active-to-polymer controls size; with insufficient polymer, nanoparticles grow too large, and with excess stabilizing polymer, micelles may form. At or above a threshold mixing intensity (Reynolds number, Re), where the mixing time is shorter than the nanoparticle growth time, nanoparticle size no longer depends on flowrate but only on stream composition.² The key to the mixing is turbulence, which is scalable, and which is fundamentally different than the flows with microfluidics devices, which inherently involve low Reynolds numbers.

Evolution of Mixers and Scalability

The original mixer design comprised two opposing equal-momentum streams that collide in a cylindrical mixing volume. Using handheld syringes or syringe pumps to drive the streams, this confined impinging jet (CIJ) mixer allowed the production of

small batches for rapid screening and formulation development (Figure 1). Nanoparticle size stability after formation depends on the rate of growth by Ostwald ripening, which depends on the solubility of the active in the solution phase.³ Since the CIJ mixer requires equal stream velocities, the resulting solvent:antisolvent ratio is 1:1. The antisolvent ratio, and hence active solubility, can be reduced by collecting the output of the CIJ into a quench bath. We typically use a quench bath volume to produce a final solvent concentration of 10%. Liu et al. developed a new mixer design with four mixing streams using tangential turbulent flow (Figure 1). Termed the multi-inlet vortex mixer (MIVM), each stream in the MIVM contributes independently to the micro-mixing process.⁴

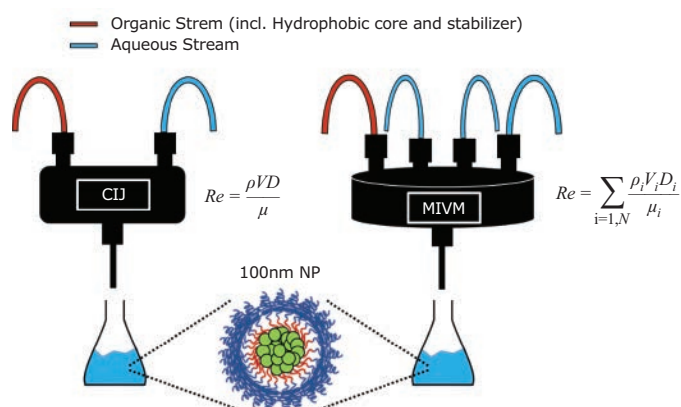


Figure 1. Schematic of the FNP process at various scales. (Left) The CIJ mixer allows for the synthesis of many small batches in rapid succession for screening formulations. (Right) The MIVM can scale up formulations to produce liters of nanoparticle solutions. (Equations for Reynolds number, Re , defined in refs. 1 and 4).

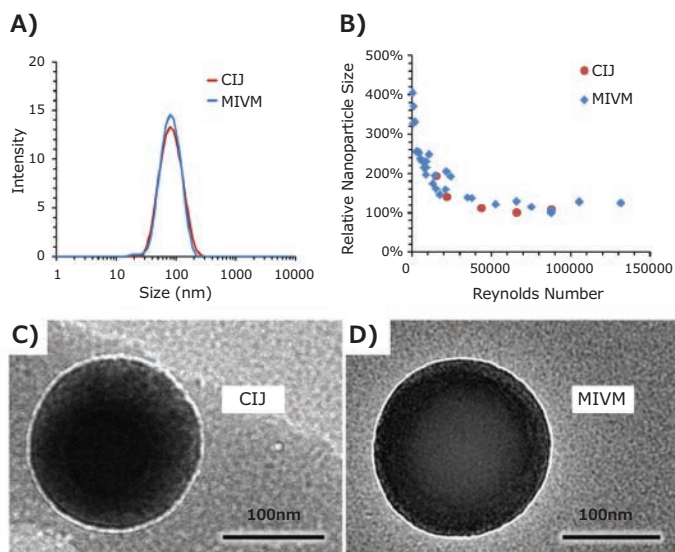


Figure 2. Comparison of nanoparticle formulations by CIJ and MIVM. **A)** DLS trace of nanoparticles formulated with Vitamin E acetate core and PS-*b*-PEG stabilizer. Nanoparticle size is independent of the mixer type. **B)** Relative nanoparticle size vs. mixing Reynolds number for CIJ and MIVM formulations. Above a threshold Reynolds number of 50000, nanoparticle size is insensitive to flow rate. **C, D)** TEM images of CIJ and MIVM nanoparticles show no significant differences between nanoparticles made by the two mixer types.

Unlike with the CIJ mixer, the momenta of the streams do not have to be matched for the MIVM, allowing for greater flexibility in nanoparticle formulations. For example, two different organic solvents can be utilized in separate streams — each containing a different API. Additionally, if sufficient dilution of the organic occurs in the mixing step, no additional quench bath is required—allowing for a truly continuous process for nanoparticle production. Markwalter et al. expanded on the MIVM design through development of a scaled-down version that required less material per batch of nanoparticles.⁵ Side-by-side comparison between the mixing devices of different scales showed no significant variation in particle size or properties as long as sufficient mixing intensity is used.⁶ Comparisons

between the MIVM and CIJ mixers show that nanoparticle sizes and distributions are identical above a threshold Re number (**Figure 2B**). Dynamic light scattering (DLS) traces and TEM images of nanoparticles formulated using the MIVM and CIJ also show no visible differences in size or properties (**Figure 2A, 2C, 2D**).⁶ This allows for a seamless development process wherein screening and small-scale formulations are performed using the CIJ mixer and then scaled up using the MIVM. A large-scale MIVM is currently being used at WuXi AppTec (Shanghai) to produce 250 nm nanoparticles of an antimalarial drug at 2 L/min in 300 L batches.

Stabilizer Selection

As mentioned previously, the amphiphilic stabilizer plays a critical role during nanoparticle formation. For the majority of FNP applications, initial screening typically uses non-degradable block copolymers. Polystyrene-*b*-polyethylene glycol (PS-*b*-PEG) is a versatile stabilizer for many applications. When incorporated into a nanoparticle, the hydrophilic PEG chains form a dense outer corona around the hydrophobic core. This dense PEG layer bestows favourable biological properties such as long circulation times and mucus penetration.⁷ Switching some or all the PEG copolymer to polyacrylic acid (PAA) or 2-(dimethylamino) ethyl methacrylate (DMEMA) can imbue the nanoparticle with negative or positive surface charges, respectively. Since surface charge affects nanoparticle biodistribution and clearance, tuning the surface charge can help target nanoparticles to specific tissues of interest. For applications requiring biodegradable nanoparticles, the polystyrene block can be swapped out for either polylactic acid (PLA) or polycaprolactone (PCL).⁸ Hydrolytic degradation of these polymers allows for slow and sustained drug release from the nanoparticles, and ultimately clearance. **Figure 3** contains the chemical structures of the commonly used block copolymer stabilizers. For global health applications, production costs dictate the use of lower cost materials during the formulation process. In these systems, more affordable stabilizers can be used, including hydroxypropyl methylcellulose acetate succinate (HPMC-AS), lecithin, zein, or casein.⁹

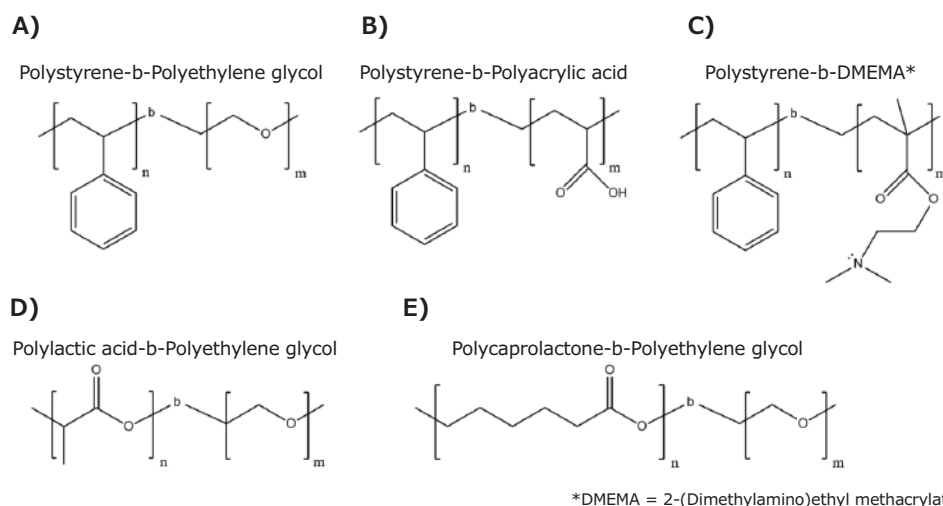


Figure 3. Typical polymeric stabilizers used for FNP. The relatively inexpensive polystyrene-based block co-polymers **A, B, C)** are generally used for prototyping or *ex-vivo* applications. Biodegradable co-polymers **D, E)** are used in therapeutic applications.

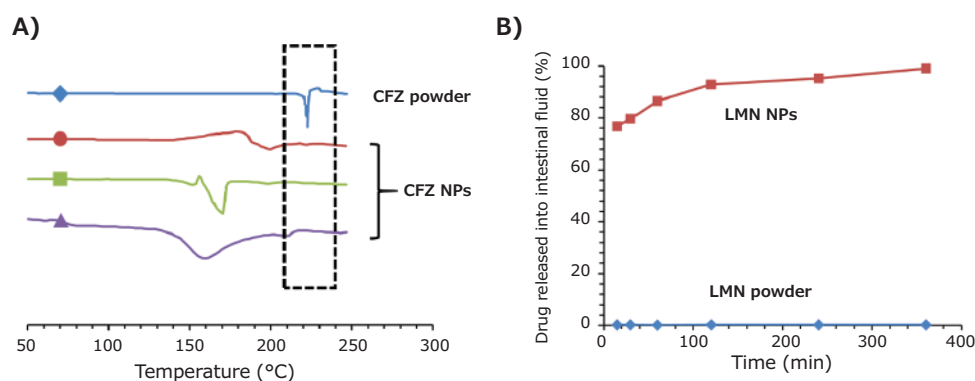


Figure 4. Applications of FNP in the encapsulation of oral therapeutics. **A)** DSC trace of three clofazimine nanoparticle formulations. CFZ powder exhibits a crystallization peak at 22 °C, while nanoparticle formulations can preserve CFZ in its amorphous state. **B)** Drug release assays of LMN formulations in simulated intestinal fluid. Nanoparticles exhibit close to full release after 2 hours while LMN powder exhibits <1% drug in solution.

Applications in Oral Delivery Formulations

One application of FNP is the encapsulation of hydrophobic drugs to improve the API's bioavailability. Clofazimine (CFZ) is a hydrophobic molecule initially used to treat leprosy but recently found to also be effective against *Cryptosporidium* infections, a leading cause of diarrhea in the developing world. However, CFZ, in its pure form, suffers from slow dissolution rates in the GI tract and is thus unsuitable for the fast-acting treatment required for *Cryptosporidium*. Flash nanoprecipitation provides enhanced solubility and improved CFZ dissolution. When encapsulated by the fast precipitation and stabilization process of FNP, the hydrophobic active molecule can be captured and preserved in an amorphous form. Additionally, the small size of FNP nanoparticles increases the specific surface area, which increases drug dissolution rate. Both factors improve the solubility and oral bioavailability of CFZ. In work performed by Zhang et al., CFZ was encapsulated into nanoparticles at very high encapsulation efficiencies (>92%) using a variety of low-cost stabilizers.⁹ DSC traces confirmed that encapsulation into nanoparticles preserved the amorphous state of CFZ (**Figure 4A**) even after processing the NPs into dry powder via spray drying or lyophilization. After incubation in simulated gastric and intestinal fluid, CFZ nanoparticles exhibited 50–90x higher supersaturation levels and complete dissolution after 6hr. Feng et al. also showed that FNP's ability to stabilize an API's amorphous form and improve dissolution was not unique to CFZ.¹⁰ Lumefantrine (LMN) is another hydrophobic API that is an effective treatment for malaria. Like clofazimine, lumefantrine also suffers from poor bioavailability and absorption in the GI tract. In the study, LMN was encapsulated into nanoparticles using low-cost natural polymers. Similar to the prior study with CFZ, FNP demonstrated the ability to suppress the crystallization of LMN and improved dissolution in simulated intestine fluid by over 2 orders of magnitude (**Figure 4B**). The amorphous nanoparticle form also decreased the difference between dissolution in fed state versus fasted state intestinal fluids. Nanoparticle formulation can decrease the sensitivity of release to environmental conditions including high temperature or humidity relative to that of traditional spray dried dispersions of the same API.¹¹

Applications in Medical Imaging

Contrast agents have commonly been used in medical diagnostics to enable more targeted and sensitive imaging. Commonly used contrast agents, such as FDG for PET, are directly injected into the patient and thus must be water-soluble. FNP enables encapsulation of water-insoluble compounds, opening the door for a variety of previously inaccessible hydrophobic contrast agents. Furthermore, the FNP process excels at generating highly loaded nanoparticles, which can drastically improve imaging sensitivity through the concentration of contrast agents in a nanoparticle core. In one example, phthalocyanine-based dyes are encapsulated at 35% core loading using PS-*b*-PEG stabilizer.¹² At these high core concentrations, nanoparticles can be used for contrast-assisted photoacoustic imaging. Lu et al. used photoacoustic imaging to investigate the biodistribution of nanoparticles in a mouse tumor model.¹³ The sharp and defined absorbance spectra of the organic dye enables multiplexed imaging, where signals are collected at various wavelengths and deconvoluted to generate a combined image. Using this technology, both nanoparticle and oxygenated/deoxygenated blood signal can be visualized simultaneously (**Figure 5A**). More conventional fluorescence imaging can also be used to track biodistribution, as shown in **Figure 5B**. In this image of gel microparticles containing fluorescent nanoparticles, microparticle size determines capture in the lungs. Pinkerton et al. expanded the diagnostic applications of FNP to MRI through the encapsulation of iron oxide-based nanocrystals (IONC).¹⁴ Since a strong T2 MRI signal is highly dependent on IONC size and density, small clusters of IONCs were formulated into nanoparticles at up to 25% wt., using FNP in a single-step assembly process. Hydroxy-terminated PS-*b*-PEG was used as the stabilizer to enhance uptake by liver macrophages. In an NSCLC orthotopic mouse model, these IONCs nanoparticles were able to enhance MRI contrast of the liver and allow detection of otherwise non-visible tumor metastases (**Figure 5C**).

The use of radiotracer-based PET or SPECT imaging can further increase sensitivity and imaging resolution.¹⁵ Synthesis of nanoparticles with the ability to "load" these tracers in a fast and efficient manner is required. One approach is to conjugate

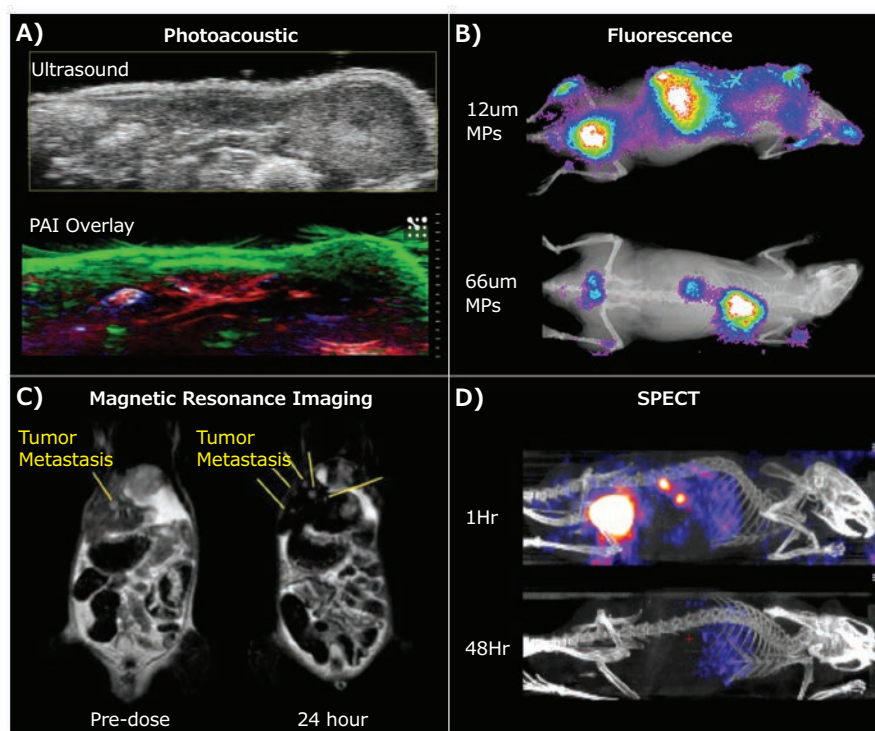


Figure 5. Biological imaging applications of FNP nanoparticles. **A)** Multiplex imaging using photoacoustic tomography of a mouse model shows nanoparticle accumulation in the skin (green). Oxygenated and deoxygenated blood can also be visualized (red and blue, respectively). **B)** Fluorescence of dye-encapsulated nanoparticles. Biodegradable microparticles containing these nanoparticles were injected into mice. Smaller particles accumulated in the liver while larger particles tracked to the lungs. **C)** MRI imaging of liver metastases in a mouse tumor model using iron oxide-based nanocrystals (IONC) encapsulated nanoparticles. Yellow lines point to the locations of liver metastases before and after injection of IONC nanoparticles. Nanoparticles persist in healthy tissues (appearing black) — generating contrast that allows better visualization of metastasis. **D)** SPECT imaging of ^{111}In labeled nanoparticles shows biodistribution and clearance profile over time.

a chelating molecule onto the hydrophilic end of the stabilizer. Radiotracers can then be captured into these chelators to form SPECT/PET-active nanoparticles. In a SPECT study, DPTA (diethylenetriaminepentaacetic acid) conjugated PS-*b*-PEG was used to chelate ^{111}In . These nanoparticles were then used in a pharmacokinetic study to quantify the clearance mechanism and rate of clearance of nanoparticles (Figure 5D). More recently, Lu et al. demonstrated a method for radiolabeling of PEG-coated nanoparticles with 64-Cu for use in PET that has advantages over surface conjugation. Encapsulation of a phthalocyanine-based metal chelator occurs first, where the very hydrophobic phthalocyanine is in the core of the nanoparticle. At a later time the nanoparticles are “PET activated”—the PET active Cu-64 is loaded into the core through a fast and straightforward incubation step.¹⁶ This core-radiolabeling minimizes potential off-target effects from having chelators exposed on the nanoparticle surface.

Applications in Targeting to Specific Cell Types

Improved targeting of nanoparticles to desired organs or cell types can both increase the effectiveness of therapeutics and the sensitivity of diagnostic imaging. This is achieved by attaching targeting ligands to the outside of nanocarriers. These targeting ligands include antibodies, peptides, sugars, and small molecules that specifically bind to a receptor on the targeted cell. In one example, mannoside-conjugated nanoparticles

were able to specifically bind to the mannose receptor of J774E macrophages (Figure 6A).¹⁷ This form of specific binding to antigen-presenting cells could expand the possibilities of nanoparticle-based vaccines. In the oncology field, FNP has been used to formulate folic acid targeted nanoparticles enabling localization to KB tumor cells (Figure 6B). In collaboration with Janssen Pharmaceuticals, Elias et al. showed that scaffold proteins based on a consensus human fibronectin domain, termed Centryrins, can also be used for nanoparticle targeted therapeutics. EGFR-targeting centryrins were functionalized onto PS-*b*-PEG nanoparticles and successfully localized to HER2 breast cancer cells (Figure 6C).

Whereas most studies formulated the nanoparticles first, then modified the nanoparticle surface, functionalization can also occur before nanoparticle formation by directly reacting the targeting ligand onto the stabilizing polymer. Modifying the polymer prior to FNP allows for precise quantification of the percentage of functionalization on the nanoparticle surface. Furthermore, tuning of the functionalized surfaces occurs by combining modified polymer with known portions of the unmodified polymer during FNP. In one example, the hormone LHRH was modified onto the end of a PS-*b*-PEG polymer and then used to formulate FNP nanoparticles with various degrees of functionalization.¹⁸ In vitro results showed strong nanoparticle uptake by MS578T breast cancer cells (Figure 6D).

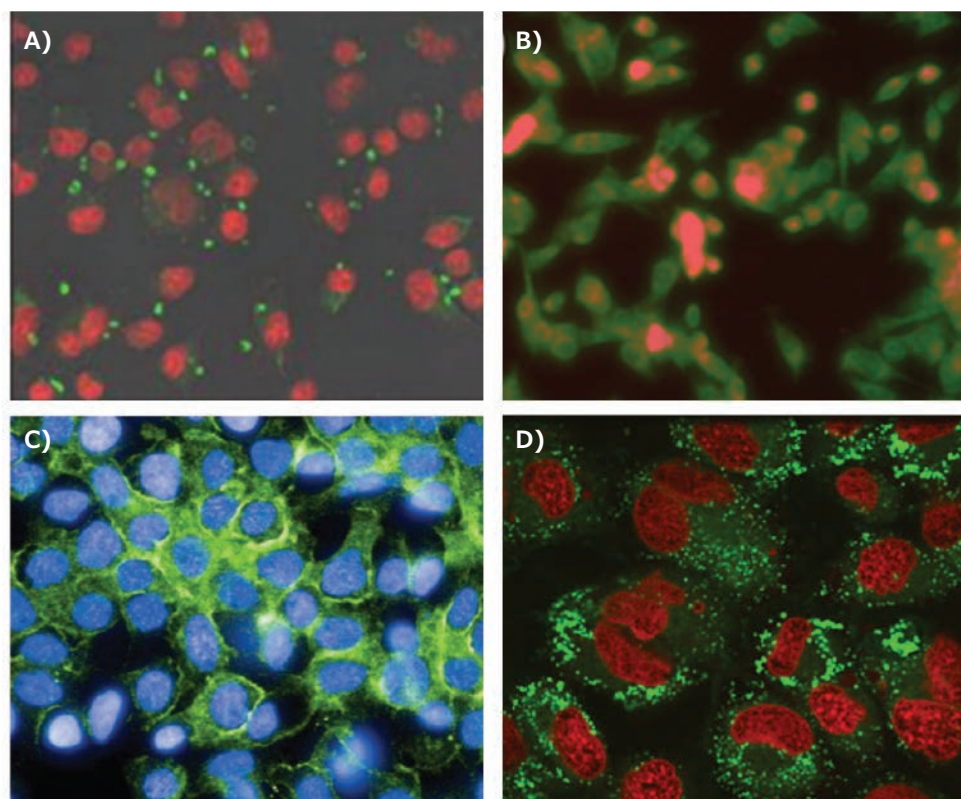


Figure 6. Targeting application of FNP nanoparticles. **A)** Mannoside-targeted nanoparticle localization to the mannose receptor of J774E macrophages. Conjugation of mannoside to the PEG outer-corona of the nanoparticles. Nanoparticles are visualized in green while cells are in red. **B)** Folic acid modified nanoparticles targeting KB tumor line cells. Nanoparticle fluorescence is shown in red while cells are stained green. **C)** Centyrin scaffold targeting EGFR receptors on HER2 line cells. **D)** Uptake of 80 nm nanoparticles with surface conjugated luteinizing hormone-releasing hormone (LHRH) into MS578T breast cancer cells. Nanoparticles and cells are visualized in green and red, respectively.

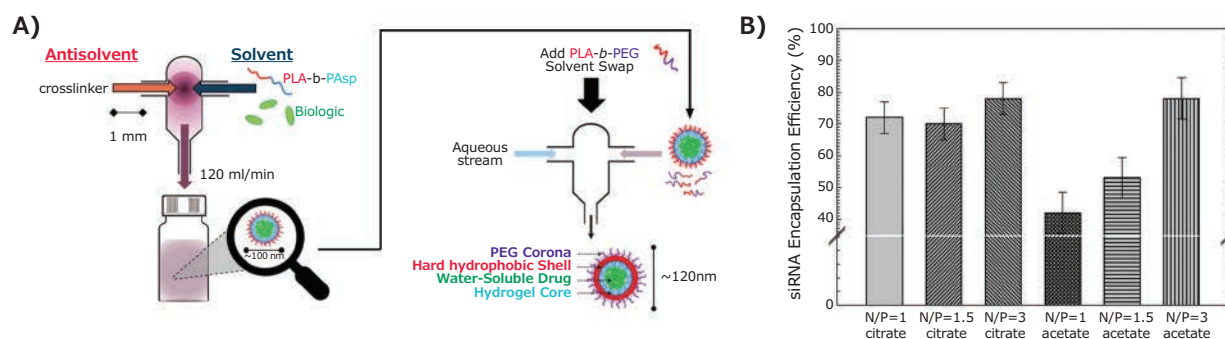


Figure 7. Encapsulation of hydrophilic actives **A)** Procedure of iFNP. Precipitation of a biologic or another hydrophilic active occurs by mixing with an organic antisolvent. The resulting inverse nanoparticle is then coated with a second polymer to form a water-dispersible nanoparticle. Reproduced with permission from reference 20, copyright 2014 ACS Publishing. **B)** Encapsulation of siRNA using charge pairing. Neutralization of anionic siRNA by cationic lipids allows for the formation of siRNA nanoparticles with very high encapsulation efficiency. Reproduced with permission from reference 21, copyright 2019 Royal Society of Chemistry.

Applications in Encapsulating Water-Soluble Actives

While FNP works well for encapsulating hydrophobic APIs with $\log P > 5$, many less hydrophobic drugs can also be encapsulated. Currently, researchers are studying two approaches to expand the capabilities of FNP to encapsulate hydrophilic APIs. In inverse Flash NanoPrecipitation (iFNP), precipitation of a hydrophilic active occurs using an organic anti-solvent stream. Unlike a traditional FNP nanoparticle, this “inverse” nanoparticle has hydrophobic ends pointing out and hydrophilic tails pointing inward. In a second

FNP coating step, a hydrophilic polymer is coated onto the iFNP nanoparticle to transfer it into an aqueous phase (Figure 7A).¹⁹ Another approach to encapsulate hydrophilic APIs involves the use of hydrophobic ion pairing (HIP). By introducing a counterion to pair with the hydrophilic API electrostatically, effectively turning off the charged groups — allowing the resulting ion-pair to precipitate during FNP. Gindy et al. utilized this method to ion-pair and encapsulate siRNA with a cationic lipid at efficiencies greater than 70% (Figure 7B).²⁰ Ristroph et al. have reviewed the encapsulation of peptides and small molecule APIs by HIP.²¹

Conclusion

Nanomedicine is ever-changing, with advances in formulation techniques and therapies. The FNP platform provides a technique to produce small-scale laboratory samples for research, and it has a straightforward path to large scale commercial production. It applies to a wide variety of actives from hydrophobic actives to soluble actives rendered hydrophobic by ion-pairing, to soluble oligonucleotides, peptides, and proteins by inverse-FNP. FNP, as a platform technology, is also continually evolving to both expand applications and to improve the process itself. This review presented only a selected sample of biomedical applications, but we hope it will open the door for more innovations in nanoparticle-based therapies and diagnostics. A video tutorial on the operation of CIJ and MIVM mixers for FNP nanoparticle formation has been published.²²

References

- (1) Johnson, B.; Prud'homme, R. *Aust. J. Chem.* **2003**, *56*, 1021–1024.
- (2) Pagels, R. F.; Edelstein, J.; Tang, C.; Prud'homme, R. K. *Nano Lett.* **2018**, *18* (2), 1139–1144.
- (3) Kumar, V.; Wang, L.; Riebe, M.; Tung, H. H.; Prud'homme, R. K. *Mol. Pharm.* **2009**, *6* (4), 1118–1124.
- (4) Liu, Y.; Cheng, C.; Liu, Y.; Prud'homme, R. K.; Fox, R. O. *Chem. Eng. Sci.* **2008**, *63* (11), 2829–2842.
- (5) Markwalter, C. E.; Prud'homme, R. K. *J. Pharm. Sci.* **2018**, *107* (9), 2465–2471.
- (6) Feng, J.; Markwalter, C. E.; Tian, C.; Armstrong, M.; Prud'homme, R. K. *J. Transl. Med.* **2019**, *17* (1), 200.
- (7) Suk, J. S.; Xu, Q.; Kim, N.; Hanes, J.; Ensign, L. M. *Adv. Drug. Deliv. Rev.* **2016**, *99* (Pt A), 28–51.
- (8) (a) Pagels, R. F.; Edelstein, J.; Tang, C.; Prud'homme, R. K. *Nano Lett.* **2018**, *18* (2), 1139–1144; (b) Gindy, M. E.; Prud'homme, R. K. *Expert Opin. Drug Del.* **2009**, *6* (8), 865–878.
- (9) Zhang, Y.; Feng, J.; McManus, S. A.; Lu, H. D.; Ristroph, K. D.; Cho, E. J.; Dobrijevic, E. L.; Chan, H.-K.; Prud'homme, R. K. *Mol. Pharm.* **2017**, *14* (10), 3480–3488.
- (10) Feng, J.; Zhang, Y.; McManus, S. A.; Qian, R.; Ristroph, K. D.; Ramachandruni, H.; Gong, K.; White, C. E.; Rawal, A.; Prud'homme, R. K. *Soft Matter* **2019**, *15* (11), 2400–2410.
- (11) Pansare, V. J.; Rawal, A.; Goodwin, A.; Beyerinck, R.; Prud'homme, R. K.; Friesen, D. T.; Grass, M.; Muske-Dukes, A.; Vodak, D. T. *Mol. Pharm.* **2018**, *15* (2), 495–507.
- (12) Lu, H. D.; Lim, T. L.; Javitt, S.; Heinmiller, A.; Prud'homme, R. K. *ACS Comb. Sci.* **2017**, *19* (6), 397–406.
- (13) Lu, H. D.; Wilson, B. K.; Heinmiller, A.; Faenza, B.; Hejazi, S.; Prud'homme, R. K. *ACS Appl. Mater. Inter.* **2016**, *8* (23), 14379–14388.
- (14) Pinkerton, N. M.; Gindy, M. E.; Calero-DdelC, V. L.; Wolfson, T.; Pagels, R. F.; Adler, D.; Gao, D.; Li, S.; Wang, R.; Zevon, M.; Yao, N.; Pacheco, C.; Therien, M. J.; Rinaldi, C.; Sinko, P. J.; Prud'homme, R. K. *Adv. Health. Mater.* **2015**, *4* (9), 1376–1385.
- (15) Tang, C.; Edelstein, J.; Mikitsch, J. L.; Xiao, E.; Hemphill, A. H., 2nd; Pagels, R.; Chacko, A.-M.; Prud'homme, R. *J. Mater. Chem. B* **2016**, *4* (14), 2428–2434.
- (16) Lu, H. D.; Wang, L. Z.; Wilson, B. K.; McManus, S. A.; Juma'an, J.; Padakanti, P. K.; Alavi, A.; Mach, R. H.; Prud'homme, R. K. *ACS Appl. Mater. Inter.* **2018**, *10* (4), 3191–3199.
- (17) D'Addio, S. M.; Baldassano, S.; Shi, L.; Cheung, L.; Adamson, D.; Bruzek, M.; Anthony, J.; Laskin, D.; Sinko, P.; Prud'homme, R. *J. Control. Release* **2013**, *168* (1), 41–49.
- (18) Akbulut, M.; Ginart, P.; Gindy, M.; Theriault, C.; Chin, K.; Soboyejo, W.; Prud'homme, R. *Adv. Funct. Mater.* **2009**, *19*, 718–725.
- (19) Markwalter, C. E.; Pagels, R. F.; Hejazi, A. N.; Gordon, A. G. R.; Thompson, A. L.; Prud'homme, R. K. *AAPS* **2020**, *22* (2), 18.
- (20) Gindy, M. E.; DiFelice, K.; Kumar, V.; Prud'homme, R. K.; Celano, R.; Haas, R. M.; Smith, J. S.; Boardman, D. *Langmuir* **2014**, *30* (16), 4613–4622.
- (21) Ristroph, K. D.; Prud'homme, R. K. *Nanoscale Adv.* **2019**, *1* (11), 4207–4237.
- (22) Markwalter, C. E.; Pagels, R. F.; Wilson, B. K.; Ristroph, K. D.; Prud'homme, R. K. *J. Vis. Exp.* **2019**, 143, e58757.

NanoFabTx™

Name	Description	Kit Components	Cat. No.
NanoFabTx™ PLGA-Nano, for synthesis of 100–200 nm particles	Reagent kit for the synthesis of 100–200 nm nanoparticles	PLGAStabilizer	909637–1KT
NanoFabTx™ PLGA-Micro, for synthesis of 1–5 μm particles	Reagent kit for the synthesis of 1–5 μm microparticles	PLGAStabilizer	912212–1KT
NanoFabTx™ PLGA-Micro, for synthesis of 10–30 μm particles	Reagent kit for the synthesis of 10–30 μm microparticles	PLGAStabilizer	912220–1KT
NanoFabTx™ Materials screening kit, for synthesis of PEGylated polymeric nanoparticles	Reagent kit for the screening of optimal polymers for PEGylated nanoparticle formulation	PEGylated PLGA, PLA, and PCLStabilizer	915408–1KT
NanoFabTx™ preclinical materials screening kit, for synthesis of polymeric nanoparticles	Reagent kit for the screening of optimal polymers for nanoparticle formulation	EXPANSORB® PLGA and PLA Stabilizer	915149–1KT
NanoFabTx™ PLA-Nano, for synthesis of 100–200 nm particles	Reagent kit for the synthesis of 100–200 nm nanoparticles	PLA Stabilizer	978075–1KT
NanoFabTx™ Microfluid - Nano, device kit	Microfluid device kit for synthesis of nanoparticles	Microfluid chip Tubing and accessories	911593–1KT
NanoFabTx™ Microfluid - Micro, device kit for synthesis of 1–5 μm particles	Microfluid device kit for synthesis of 1–5 μm particles	Microfluid chip Tubing and accessories	911860–1KT
NanoFabTx™ Microfluid - Micro, device kit for synthesis of 10–30 μm particles	Microfluid device kit for synthesis of 10–30 μm particles	Microfluid chip Tubing and accessories	911879–1KT

Biodegradable Polymers

Poly(lactide-co-glycolide)

Name	Lactide:Glycolide	Mol. Wt./Viscosity	Cat. No.
Poly(D,L-lactide- <i>b</i> -glycolide) lactide:glycolide	75:25	average M _n 12,000	908525-100MG
Poly(D,L-lactide- <i>b</i> -glycolide) lactide:glycolide	50:50	viscosity 0.035 dL/g	908533-100MG
Poly(lactide-co-glycolide)-fluorescein	50:50	M _n 10,000-20,000	908649-50MG
4arm-poly(lactide-co-glycolide)	55:45	M _n 38,000-60,000	909904-500MG
3arm-poly(lactide-co-glycolide)	55:45	M _n 38,000 -60,000	909912-500MG

Biodegradable Diblock Copolymers

Poly(ethylene glycol)-*block*-poly(lactide-*co*-glycolide)

Name	Structure	Molecular Weight	Cat. No.
Poly(ethylene glycol) methyl ether- <i>block</i> -poly(lactide- <i>co</i> -glycolide)		PEG average M_n 2,000 PLGA average M_n 10,000	913138-1G
		PEG average M_n 5,000 PLGA average M_n 5,000	911429-1G
		PEG average M_n 5,000 PLGA average M_n 10,000	911410-1G
		PEG average M_n 2,000 PLGA average M_n 10,000	911399-1G
Biotin-poly(ethylene glycol)- <i>b</i> -poly(lactide- <i>co</i> -glycolide)		PEG average M_n 2,000 PLGA average M_n 10,000	909882-50MG

Poly(ethylene glycol)-*block*-poly(ε-caprolactone)

Name	Structure	Molecular Weight	Cat. No.
Poly(ethylene glycol)- <i>block</i> -poly(ε-caprolactone) methyl ether		PCL average M_n ~13,000 PEG average M_n ~5,000 average M_n ~18,000 (total)	570311-250MG 570311-1G
		PCL average M_n ~5,000 PEG average M_n ~5,000 average M_n ~10,000 (total)	570303-250MG 570303-1G

Functionalized Biodegradable Diblock Copolymers

Poly(ethylene glycol)-*block*-poly(D,L lactide)

Name	Structure	Molecular Weight	Cat. No.
Carboxylic acid-poly(ethylene glycol)- <i>b</i> -poly(D,L lactide)		PDLA average M_n 55,000 PEG average M_n 5,000	909289-100MG
		PDLA average M_n 16,000 PEG average M_n 5,000	909300-100MG
N-Hydroxysuccinimide ester-poly(ethylene glycol)- <i>b</i> -poly(D,L lactide)		PDLA average M_n 55,000 PEG average M_n 5,000	909297-100MG
		PDLA average M_n 16,000 PEG average M_n 5,000	909874-100MG

Poly(ethylene glycol)-*block*-poly(lactide-*co*-glycolide)

Name	Structure	Molecular Weight	Cat. No.
Carboxylic acid-poly(ethylene glycol)- <i>b</i> -poly(lactide- <i>co</i> -glycolide)		PEG average M_n 5,000 PLGA average M_n 20,000	909858-100MG
Folate-poly(ethylene glycol)- <i>b</i> -poly(lactide- <i>co</i> -glycolide)		PEG average M_n 2,000 PLGA average M_n 10,000	909769-50MG

Poly(ethylene glycol)-*block*-poly(ε-caprolactone)

Name	Structure	Molecular Weight	Cat. No.
Allyl-poly(ethylene glycol)- <i>b</i> -poly(ε-caprolactone)		PCL average M_n 5,000 PEG average M_n 5,000	901844-1G

Name	Structure	Molecular Weight	Cat. No.
Amine-poly(ethylene glycol)- <i>b</i> -poly(ϵ -caprolactone)		PCL average M_n 5,000 PEG average M_n 5,000	904740-500MG
Carboxylic acid-poly(ethylene glycol)- <i>b</i> -poly(ϵ -caprolactone)		PCL average M_n 5000 PEG average M_n 5000	901702-500MG
<i>N</i> -Hydroxysuccinimide ester-poly(ethylene glycol)- <i>b</i> -poly(ϵ -caprolactone)		PCL average M_n 5,000 PEG average M_n 5,000	901841-500MG
Pyridyl disulfide-poly(ethylene glycol)- <i>b</i> -poly(ϵ -caprolactone)		PCL average M_n 5000 PEG average M_n 5000	901910-500MG
Thiol-poly(ethylene glycol)- <i>b</i> -poly(ϵ -caprolactone)		PCL average M_n 5000 PEG average M_n 5000	901708-500MG

Trimethyl Chitosan

Name	Description	Appearance	Cat. No.
Trimethyl chitosan	degree of quaternization > 70% high molecular weight	light yellow	912034-1G
	degree of quaternization: 40- 60% medium molecular weight	light yellow	912123-1G
	degree of quaternization > 70% low molecular weight	light yellow	912700-1G

Polystyrene-*block*-poly(acrylic acid)

Name	Structure	Molecular Weight	Cat. No.
Polystyrene- <i>block</i> -poly(acrylic acid), DDMAT terminated		M_n 4,000-6,000 (poly(acrylic acid)) M_n 2,700-3,300 (polystyrene)	776351-500MG
Polystyrene- <i>block</i> -poly(acrylic acid)		M_n 1,000-2,000 (poly(acrylic acid)) M_n 27,000-31,000 (polystyrene) M_n 28,000-33,000 (total)	747009-500MG
		M_n 27,000-33,000 (polystyrene) M_n 7,000-9,000 (poly(acrylic acid)) M_n 34,000-42,000 (total)	746983-500MG
		M_n 31,000-37,000 (total) M_n 4,000-6,000 (poly(acrylic acid)) M_n 27,000-31,000 (polystyrene)	746991-1G
Polystyrene- <i>block</i> -poly(acrylic acid), azide terminated		M_n 8,100-9,100 M_n 2,600-2,950 (polyacrylic acid) M_n 5,500-6,000 (polystyrene) average M_n 8,600	757594-250MG
		M_n 8,100-9,100 M_n 1,600-1,950 (poly(acrylic acid)) M_n 6,500-7,000 (polystyrene) average M_n 8,700	735892-250MG

EVERYTHING BUT THE KITCHEN SINK

Comprehensive biodegradable polymers for drug delivery

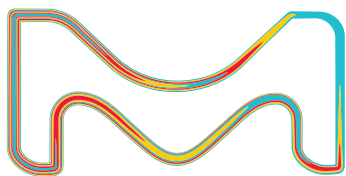
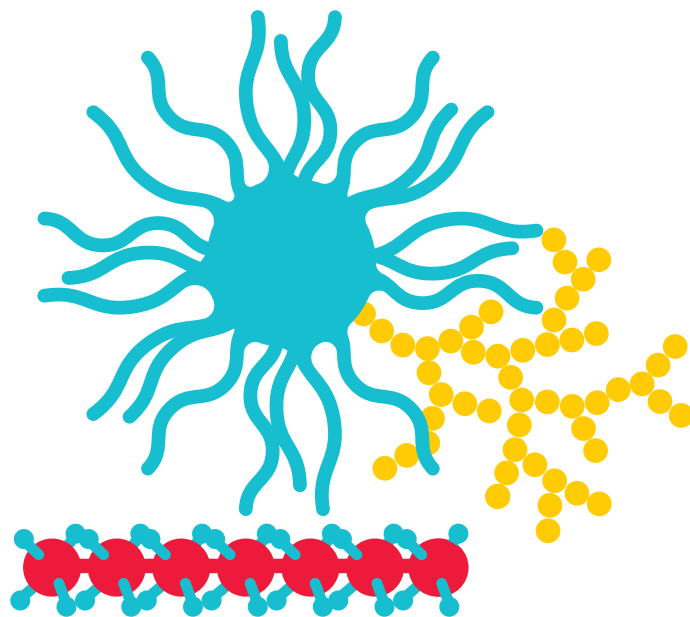
Biodegradable polymers contain polymer chains that are hydrolytically or enzymatically cleavable, resulting in biocompatible or nontoxic by-products. They are widely used in drug delivery research to achieve controlled and targeted delivery of therapeutic agents (e.g. APIs, genetic material, peptides, vaccines, and antibiotics).

We now offer the following classes of high-purity biodegradable polymers:

- Poly (lactide-co-glycolide) copolymers (PLGA)
- Poly(lactic acid) (PLA)
- Poly(caprolactone) (PCL)
- Amphiphilic block copolymers
- End-functionalized biodegradable polymers

For more information, please visit:

[SigmaAldrich.com/resomer](https://www.sigmaaldrich.com/resomer)



The life science
business of Merck
operates as
MilliporeSigma in
the U.S. and Canada.

Sigma-Aldrich[®]
Lab & Production Materials

Recent Progress on Nonviral Delivery Carriers for CRISPR/Cas9 Systems



Chun Wang,[†] Zhanzhan Zhang,[†] and Yang Liu^{*}

State Key Laboratory of Medicinal Chemical Biology, Key Laboratory of Functional Polymer Materials of Ministry of Education, College of Chemistry, Nankai University, National Demonstration Center for Experimental Chemistry Education, Nankai University, Tianjin, 300071, China.

^{*}E-mail: yliu@nankai.edu.cn

[†]Contributed equally in this work.

Introduction

The CRISPR/Cas9 system has recently emerged as a robust and versatile genome-editing platform for building disease models and correcting diseased genes. CRISPR stands for and refers to clustered regularly interspaced short palindromic repeat found by Nakata et al. in 1987¹ as repeat sequences interspaced by nucleotide spacers in the *Escherichia coli* genome. This genome-editing system contains two main components: a nuclease protein Cas9 that binds to DNA and initiates double-strand breaks (DSBs), and a very short single guide RNA (sgRNA) that directs the Cas9 nuclease to the targeted genomic locus. Since the CRISPR/Cas9 system can only function within the cellular environment, this genome-editing system requires a delivery mechanism to targeted cells. To date, both physical approaches and viral vectors have been extensively studied for CRISPR/Cas9 delivery, showing significant progress in improving delivery accuracy and transfection efficiency. However, these methods have intrinsic limitations, including insertional mutagenesis, carcinogenesis, and immunogenicity, that dramatically restrict their clinical applications. Therefore, new systems for CRISPR/Cas9 delivery are needed to allow the safe and effective clinical development and applications of CRISPR/Cas9 systems.

To achieve effective *in vivo* delivery of the CRISPR/Cas9 system, it is necessary to understand and overcome the three major obstacles to the use of CRISPR/Cas9 from *in vitro* loading to *in vivo* delivery. First, the size of the CRISPR/Cas9 system is more substantial than traditional gene editing tools. In detail, the

total plasmid size is larger than 7 kb, and commonly used Cas9 proteins are about 160 kDa, significantly increasing the difficulty of *in vivo* delivery. Thus, it is essential to condense the CRISPR/Cas9 system into relatively small particles through the use of suitable carriers. Second, the naked CRISPR/Cas9 genome-editing cargos are exogenous biomacromolecules, that are vulnerable to recognition and rapid clearance by the host immune system. As a result, their half-life is too short to function *in vivo*. To prolong the half-life, the delivery platform must protect the genome-editing cargo from degradation from the physiological environment. Third, the gene editing process takes place in the cytoplasm or nucleus, but the genome-editing cargos cannot readily traverse the hydrophobic lipid cell membrane by themselves. Therefore, a suitable delivery vector is required to allow the CRISPR/Cas9 system to penetrate the host cells.

In previous studies, nonviral nanoparticles like liposomes, polymeric nanoparticles, and inorganic nanoparticles have demonstrated many advantages such as lower immunogenicity, high packaging capability, and design flexibility, showing great potential to satisfy the requirements for CRISPR/Cas9 delivery. Numerous researches have recently focused on nonviral approaches as promising alternatives in developing an effective CRISPR/Cas9 delivery system. In this review, we provide an overview of the latest nonviral approaches adopted for CRISPR/Cas9 delivery in order to offer a reference for future research.

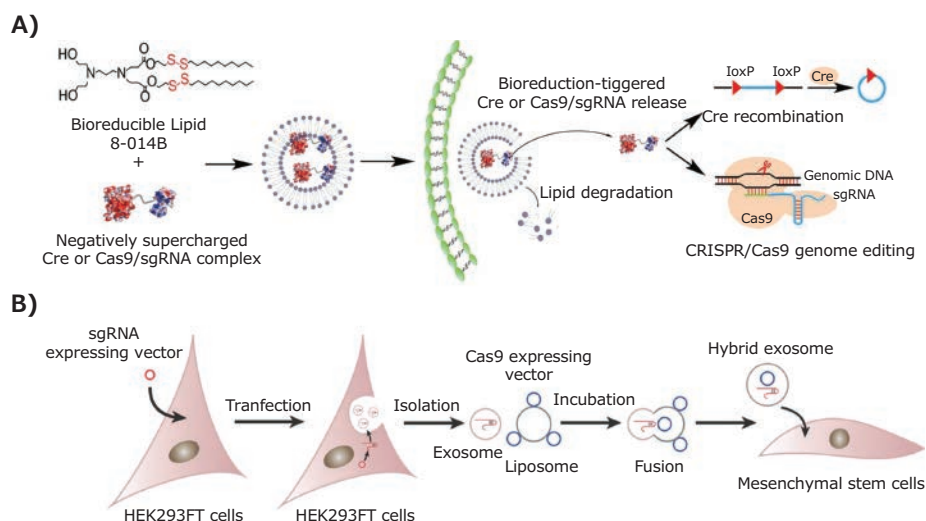


Figure 1. Lipid-based platforms. **A)** Molecular design of bioreducible lipid and its delivery mechanism. Reproduced with permission from reference 2, copyright 2016 National Academy of Science. **B)** Illustration of the procedure of how the hybrid exosomes deliver the CRISPR/Cas9 interference system. Reprinted with permission from reference 3, copyright 2018 Wiley VCH.

Lipid-Based Platforms

Lipid-based carriers are a primary type of nonviral gene carrier. Lipofectamine, a commercially available liposome, has been widely used *in vitro* for the transfection of mRNA due to its high transfection efficiency. However, the high toxicity and inflammatory side effects have limited its further application. Researchers are engaged in modifying conventional liposomes with biodegradable chemical bonds or targeting ligands to provide more functionality. Wang et al.² reported a combinatorial library of cationic bioreducible lipids to deliver Cas9/sgRNA. These lipid-based vectors can effectively facilitate the escape of Cas9/sgRNA from endosomal and direct protein to its intracellular targets under a reductive intracellular environment with more than 70% delivery efficiency (**Figure 1A**). Finn et al.³ designed a biodegradable lipid-based formulation via labile ester linkages. With the introduction of apolipoprotein E (ApoE) as the target moiety, this biodegradable lipid-based CRISPR/Cas9 vectors exhibit significantly enhanced uptake by hepatocytes cells and demonstrate more than 97% gene knockdown efficiency.

Exosomes are small extracellular vesicles secreted by mammalian cells, which can be used as attractive nanocarriers owing to their stability, biocompatibility, low immunogenicity, and low toxicity. However, it is challenging to encapsulate large nucleic acids or proteins into exosomes due to their small size (30–100 nm). To utilize the advantages of exosomes in CRISPR/Cas9 delivery, Lin et al.⁴ developed a hybrid exosome by incubating them together with liposome. Different from the original exosomes, the hybrid encapsulated CRISPR/Cas9 plasmid DNA and efficiently expressed the encapsulated genes in mesenchymal stem cells (MSCs) (**Figure 1B**).

Polymer-Based Platforms

Polymer-based nanoparticles are widely used for delivering various types of nucleic acids, including plasmid DNA, RNA, and oligonucleotide, due to their excellent encapsulation capability, specific targeting of tissues or organs, and remarkable properties in stabilizing nucleic acids against serum-induced aggregation. Based on previous research, polymer-based platforms for CRISPR/Cas9 delivery has attracted much attention.

Polyethyleneimine (PEI) is the most common polymeric gene vector. The rich amine groups of PEI endow them with high charge density, which allows efficient DNA condensation and endo/lysosomal escaping. Nowadays, PEI 25K is even considered the gold standard for DNA/RNA transfection. However, excessively strong positive charge and significant cytotoxicity limit further *in vivo* applications. Fortunately, recent research has shown that this cytotoxicity can be effectively reduced using linear and lower molecular weight PEI or by chemical modification with moieties such as PEG. Wei and colleagues⁵ reported a multifunctional nucleus-targeting “core-shell” artificial virus (RRPHC) for delivery of the CRISPR/Cas9 system. The RRPHC artificial virus has a core-shell structure, in which the core composition contains fluorinated low molecular weight PEI, and the shell formation occurs using a versatile multifunctional PEG layer (RGD-R8-PEG-HA, RRPH, **Figure 2A**). This artificial virus effectively directs the endosomal escape and nucleus entry of the CRISPR/Cas9 system without further addition of any nuclear-localization signal, exhibiting very high transfection efficiency to SKOV3 cells (more than 90%).

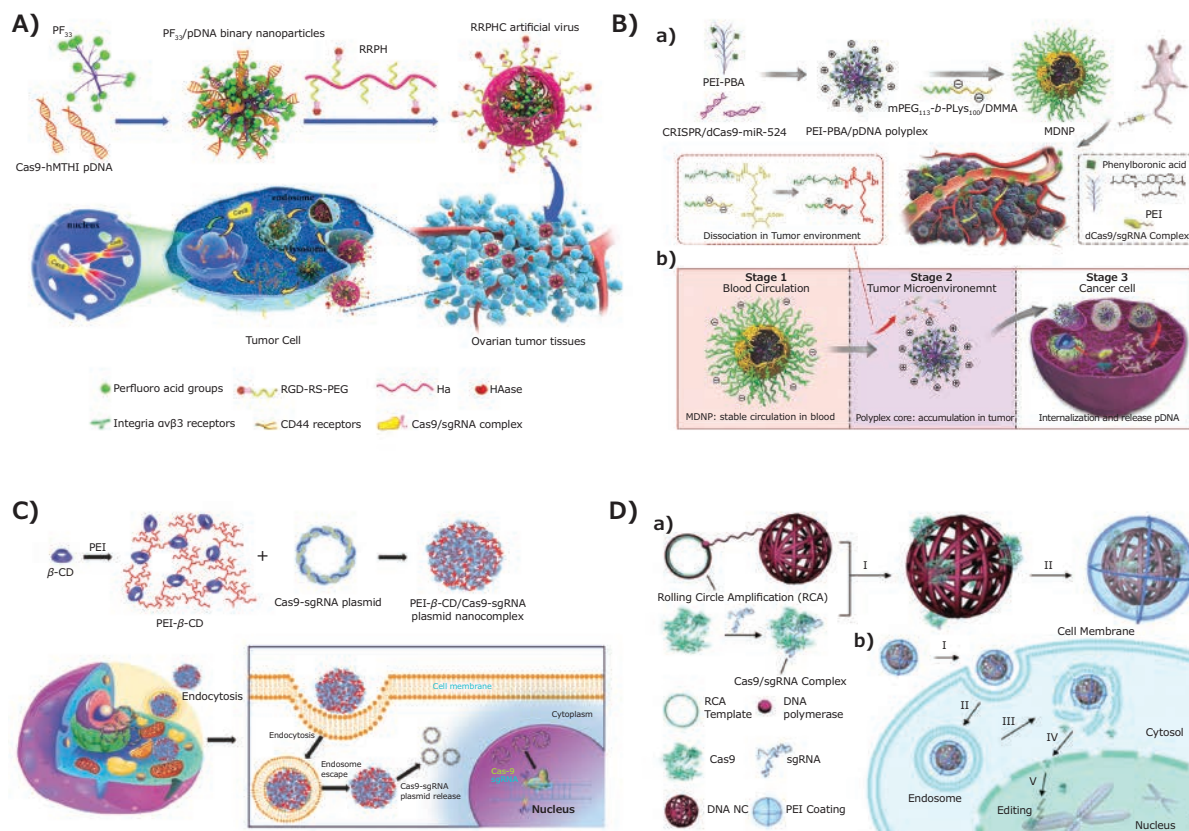


Figure 2. Polymer-based platforms. **A)** Design of the multifunctional “core-shell” artificial virus (RRPHC) for delivery of the CRISPR/Cas9 system. Reproduced with permission from reference 5, copyright 2017 American Chemical Society. **B)** Preparation of MDNP and the delivery of CRISPR/dCas9 system after intravenous injection. Reproduced with permission from reference 6, copyright 2018 American Chemical Society. **C)** Schematic illustration of PC-mediated Cas9/sgRNA plasmid delivery for genome editing. Reproduced with permission from reference 7, copyright 2015 Wiley VCH. **D)** Design of DNA nanoclew for CRISPR/Cas9 delivery system. Reproduced with permission from reference 8, copyright 2015 Wiley VCH.

Similarly, Liu et al.⁶ developed a multistage delivery nanoparticle (MDNP), comprised of phenylboronic acid (PBA) modified low molecular weight PEI and 2,3-dimethylmaleic anhydride (DMMA)-modified mPEG₁₁₃-b-PLYS₁₀₀ (Figure 2B). The corresponding surface properties at different delivery stages ensure this multistage delivery nanoparticle achieves efficient delivery of the CRISPR/dCas9-miR-524 system. In other research, Zhang and colleagues⁷ synthesized polyethyleneimine-β-cyclodextrin (PC) as a carrier for delivering Cas9/sgRNA pDNA *in vitro*. Owing to the similar structure as high molecular weight PEI, PC serves as an efficient delivery vector with high efficiency (Figure 2C). The above three studies are all based on low molecular weight PEI with functional chemical modification. Compared with high molecular weight PEI, they show similar transfection efficiency but lower cytotoxicity, demonstrating significant potential as a safer alternative to PEI 25K.

In the last decade, new nanostructures developed from DNA, including DNA tetrahedrons, DNA origami structures, DNA nanorobots, and DNA nanoclews, have shown great potential in CRISPR/Cas9 system delivery due to their uniform size, biodegradability, and spatial addressability. In 2015, Sun et al.⁸ developed a synthetic DNA nanoclew (NC)-based carrier for the delivery of Cas9/sgRNA complexes *in vitro* and *in vivo* (Figure 2D). With the assistance of PEI and nuclear-localization-signal

peptides, DNA NCs have exhibited effective endosome escape and nucleus targeting capability, achieving much higher editing efficacy (36%) compared to the cell-penetrating peptide (CPP) based vector (9.7%).

Inorganic Nanoparticles

In recent years, rigid nanocarriers such as carbon, gold, and other nanoscale inorganic materials have performed well in many gene delivery applications due to their high surface to volume ratio, size control, and colloidal stability in a physiological environment. For example, a nanocarrier composed of cationic arginine gold nanoparticles (ArgNPs) and engineered Cas9 proteins has been reported (Figure 3A).⁹ This vector could efficiently deliver protein and nucleic acid to the cytoplasm and subsequently transport it to the nucleus, ultimately achieving up to 90 % delivery efficiency. In 2018, Alsaiahi et al.¹⁰ reported the first example of applying nanoscale metal-organic frameworks (MOFs) for CRISPR/Cas9 RNP complex delivery (Figure 3B). Nanoscale zeolitic imidazolate framework-8 (ZIF-8) successfully co-encapsulated both Cas9 protein and the negatively charged sgRNA with a high loading efficiency of 17% due to its tunable pore size. With the fast-endosomal escape and enhanced nucleus delivery, the CRISPR/Cas9 system encapsulated by ZIF-8 knocked down the gene expression of green fluorescent protein

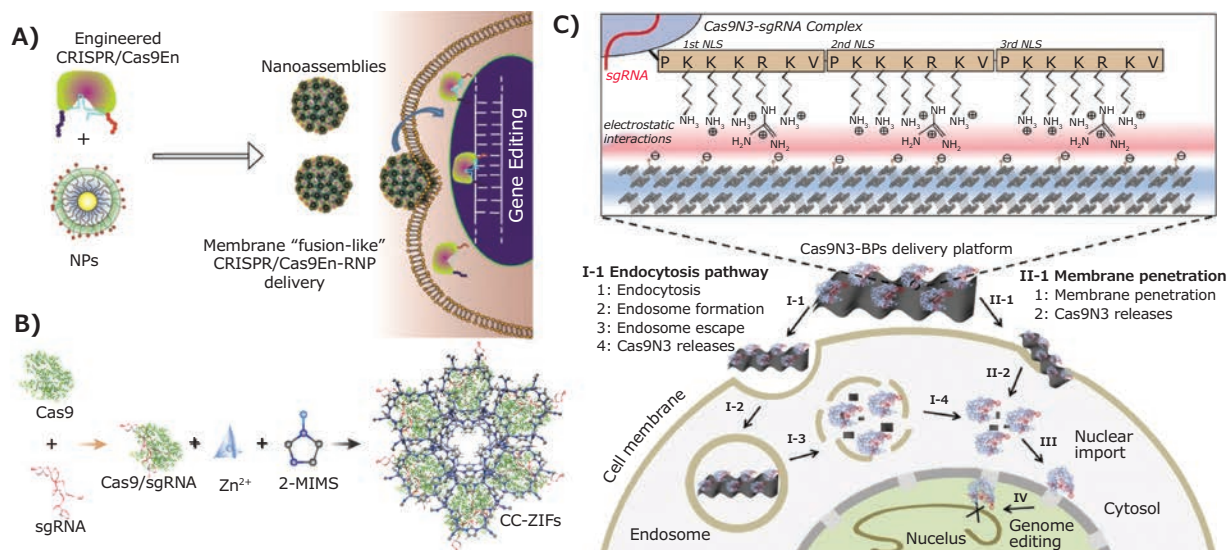


Figure 3. Inorganic Nanoparticles. **A)** Rational designing of arginine nanoparticles (ArgNPs) for effectively intracellular delivery of the Cas9 protein or Cas9-RNP. Reproduced with permission from reference 9, copyright 2017 American Chemical Society. **B)** The formation of nanoscale ZIF-8 co-encapsulating Cas9 protein and sgRNA (CC-ZIFs). Reproduced with permission from reference 10, copyright 2017 American Chemical Society. **C)** Design of the Cas9N3-BPs delivery platform and its intracellular delivery pathways. Reproduced with permission from reference 11, copyright 2018 Wiley VCH.

by 37% over 4 days. In another paper, Zhou et al.¹¹ reported the use of biodegradable two-dimensional black phosphorus nanosheets (BPs) for CRISPR/Cas9 delivery (**Figure 3C**). Cas9 RNP was loaded onto the BPs via electrostatic interaction with a remarkable loading capacity of 98.7%. The constructed delivery platform could enter the cells via both direct membrane penetration and endocytosis pathway, followed by effective endosomal escape upon biodegradation of the ultra-thin BPs. The resulting good biocompatibility and biodegradability makes it a promising topic for further research.

Hybrid Materials-Based Platforms

Like all other delivery applications, no one single carrier can solve all the problems and enable efficient CRISPR/Cas9 delivery. Combining the advantages of different materials into one hybrid multifunctional vector provides the ability to meet various needs simultaneously, ultimately achieving much more efficient delivery.

Polymeric nanoparticles coated with a SiO₂ shell have been suggested as promising hybrid carriers for safe and efficient delivery of biologically active compounds. Timin et al.¹² constructed a nanoparticle-based system by depositing poly-L-arginine hydrochloride and dextran sulfate on CaCO₃ particles using the layer-by-layer (LbL) self-assembly method. After removing the CaCO₃ core and coating with a SiO₂ shell, these carriers achieved more efficient transfection than a commercially available liposome-based transfection reagent due to its high loading capacity and biocompatibility. Liang et al.¹³ developed a PEG-PEI-Cholesterol (PPC) lipopolymer for delivering CRISPR/Cas9 plasmids (encoding VEGFA gRNA). These aptamer-functionalized PPC lipopolymers successfully decreased the VEGFA expression or secretion and demonstrated significant inhibition in orthotopic

osteosarcoma malignancy and lung metastasis. In another report, Chen et al.¹⁴ developed liposome-templated hydrogel nanoparticles (LHNPs) for targeted CRISPR/Cas9 delivery. The PEI-based hydrogel has a core-shell structure, in which the core is a cationic polyplex constructed by crosslinking cyclodextrin (CD)-engrafted PEI (PEI-CD) with adamantine (AD)-engrafted PEI (PEI-AD), whereas the shell is DOTAP lipids (**Figure 4A**). This unique core-shell structure is capable of delivering Cas9 protein and plasmid DNA simultaneously, exhibiting high delivery efficiency and low toxicity.

Graphene oxide (GO) has attracted significant attention in biological applications, especially as a carrier for the delivery of small molecular drugs and nucleic acids into cells. Compared with other nanocarriers, the planar structure of GO provides a higher specific surface area, thereby effectively enhancing the payload capacity. In 2018, Yue et al.¹⁵ developed the first delivery platform based on PEG and PEI dual-functionalized GO, which is capable of loading Cas9/sgRNA by physical adsorption and π -stacking interactions. This nanoplatform successfully achieved intracellular delivery of Cas9/sgRNA via endocytosis, exhibiting 39% gene disruption with excellent biocompatibility. (**Figure 4B**).

Also, researches have shown that hybrid multifunctional vectors are more intelligent, which can overcome both intracellular and extracellular barriers at the same time. For example, Harashima et al.¹⁶ developed a multifunctional envelope-type nanodevice (MEND) composed of a mitochondria targeting liposome called MITOPorter and enzymatically cleavable PEG (**Figure 4C**). Such intelligent nanocarriers have the potential to avoid host immune system recognition during blood circulation and realize effective cell internalization after accumulating in tumor tissues, finally achieving high delivery efficiency. Wang et al.¹⁷ created a photothermal-activatable lipid/gold nanoparticle

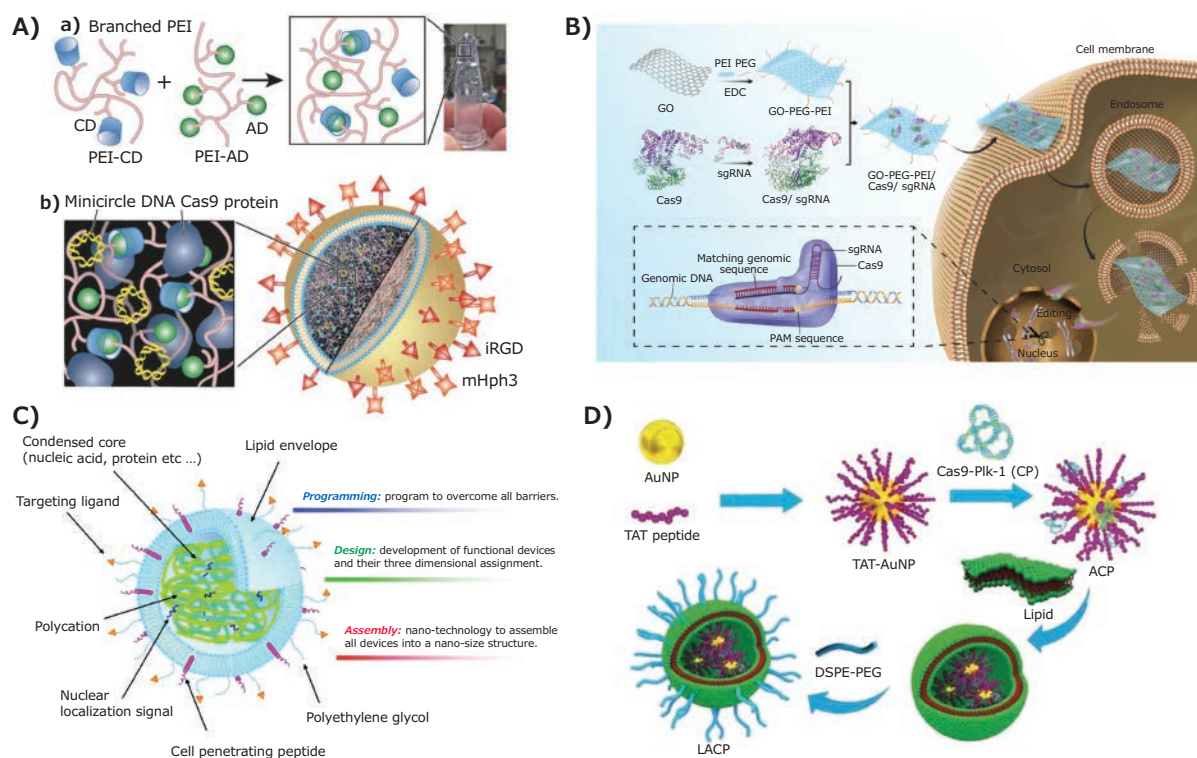


Figure 4. Delivery platforms based on hybrid materials. **A)** Formation of liposome-templated hydrogel nanoparticles (LHNPs) by DOTAP liposomes and PEI hydrogel. Reproduced with permission from reference 14, copyright 2017 Wiley VCH. **B)** The schematic process of preparation and intracellular delivery of GO-PEG-PEI based Cas9/sgRNA delivery. Reproduced with permission from reference 15, copyright 2018 Royal Society of Chemistry. **C)** Design of the multifunctional envelope-type nanodevice (MEND) based on “Programmed Packaging”. Reproduced with permission from reference 16, copyright 2012 American Chemical Society. **D)** Preparation processes for lipid-encapsulated TAT peptide-modified AuNPs. Reproduced with permission from reference 17, copyright 2017 Wiley VCH.

(AuNP) platform for the delivery of Cas9-gPlk-1 plasmids (Figure 4D). The multifunctional vehicle enters tumor cells and releases the Cas9-gPlk-1 plasmids into the cytosol by laser-triggered thermo-effects of the AuNPs. Then, by TAT guidance, the Cas9-gPlk-1 plasmids enter the nuclei to finish the gene editing. The synergistic effects of AuNPs, TAT peptide, and the outer lipid shell guarantee high efficiency and targeted gene editing.

Conclusion and Perspectives

The CRISPR/Cas9 system offers significant advantages over other genome-editing technologies such as simplicity and versatility. However, their clinical application mainly relies on the effective delivery of genome-editing cargo to the target cells. Numerous innovative nanoparticle delivery systems like polymer-based, lipid-based, and rigid inorganic nanoparticles have been designed for the CRISPR/Cas9 system. To meet the various needs of the different delivery stages *in vivo*, hybrid multifunctional delivery platforms are also in development. All these make the clinical application of nonviral vectors for CRISPR/Cas9 delivery very promising in the near future.

To date, the design of most delivery platforms are for pDNA or mRNA. Compared with the above two delivery modes, direct delivery of Cas9 protein/sgRNA shows the advantages of rapid action, high efficiency, and lower off-target effect. However, packaging RNP into a small particle while maintaining its

biological activity in the blood is still a significant challenge to overcome. Since there are few alternative protein carriers for delivery, this is a fertile research direction that is greatly needed to advance CRISPR/Cas9 technology.

Acknowledgments

This work was supported by the National Key Research and Development Programs of China (2018YFA0209700), National Natural Science Foundation of China (NSFC; Grant Nos. 51673100), the Fundamental Research Funds for the Central Universities (Nankai University; Grant Nos. ZB19100123).

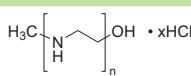
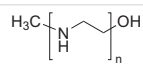
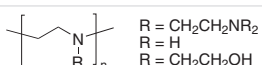
References

- (1) Ishino, Y.; Shinagawa, H.; Makino, K.; Amemura, M.; Nakata, A. *J. Bacteriol.* **1987**, *169* (12), 5429–5433.
- (2) Wang, M.; Zuris, J. A.; Meng, F.; Rees, H. A.; Sun, S.; Deng, P.; Han, Y.; Gao, X.; Pouli, D.; Wu, Q. *Proc. Natl. Acad. Sci. USA* **2016**, *113* (11), 2868–2873.
- (3) Finn, J. D.; Smith, A. R.; Patel, M. C.; Shaw, L.; Youniss, M. R.; van Heteren, J.; Dirstine, T.; Ciullo, C.; Lescaarbeu, R.; Seitzer, J.; Shah, R. R.; Shah, A.; Ling, D.; Growe, J.; Pink, M.; Rohde, E.; Wood, K. M.; Salomon, W. E.; Harrington, W. F.; Dombrowski, C.; Strapps, W. R.; Chang, Y.; Morrissey, D. V. *Cell Rep.* **2018**, *22* (9), 2227–2235.
- (4) Lin, Y.; Wu, J.; Gu, W.; Huang, Y.; Tong, Z.; Huang, L.; Tan, J. *Adv. Sci.* **2018**, *5* (4), 1700611.
- (5) Li, L.; Song, L.; Liu, X.; Yang, X.; Li, X.; He, T.; Wang, N.; Yang, S.; Yu, C.; Yin, T.; Wen, Y.; He, Z.; Wei, X.; Su, W.; Wu, Q.; Yao, S.; Gong, C.; Wei, Y. *ACS Nano* **2017**, *11* (1), 95–111.
- (6) Liu, Q.; Zhao, K.; Wang, C.; Zhang, Z.; Zheng, C.; Zhao, Y.; Zheng, Y.; Liu, C.; An, Y.; Shi, L.; Kang, C.; Liu, Y. *Adv. Sci.* **2019**, *6* (1), 1801423.

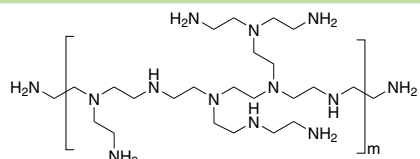
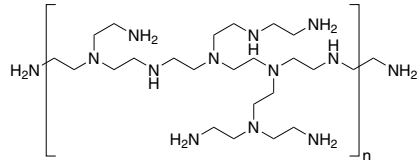
- (7) Zhang, Z.; Wan, T.; Chen, Y.; Chen, Y.; Sun, H.; Cao, T.; Songyang, Z.; Tang, G.; Wu, C.; Ping, Y.; Xu, F. J.; Huang, J. *Macromol. Rapid Commun.* **2019**, *40* (5), 1800068.
- (8) Sun, W.; Ji, W.; Hall, J. M.; Hu, Q.; Wang, C.; Beisel, C. L.; Gu, Z. *Angew. Chem.* **2015**, *54* (41), 12029-12033.
- (9) Mout, R.; Ray, M.; Yesilbag Tonga, G.; Lee, Y. W.; Tay, T.; Sasaki, K.; Rotello, V. M. *ACS Nano* **2017**, *11* (3), 2452-2458.
- (10) Alsaiani, S. K.; Patil, S.; Alyami, M.; Alamoudi, K. O.; Aleisa, F. A.; Merzaban, J. S.; Li, M.; Khashab, N. M. *J. Am. Chem. Soc.* **2018**, *140* (1), 143-146.
- (11) Zhou, W.; Cui, H.; Ying, L.; Yu, X. *Angew. Chem.* **2018**, *57* (32), 10268-10272.
- (12) Timin, A. S.; Muslimov, A. R.; Lepik, K. V.; Epifanovskaya, O. S.; Shakirova, A. I.; Mock, U.; Riecken, K.; Okilova, M. V.; Sergeev, V. S.; Afanasyev, B. V.; Fehse, B.; Sukhorukov, G. B. *Nanomedicine* **2018**, *14* (1), 97-108.
- (13) Liang, C.; Li, F.; Wang, L.; Zhang, Z. K.; Wang, C.; He, B.; Li, J.; Chen, Z.; Shaikh, A. B.; Liu, J.; Wu, X.; Peng, S.; Dang, L.; Guo, B.; He, X.; Au, D. W. T.; Lu, C.; Zhu, H.; Zhang, B. T.; Lu, A.; Zhang, G. *Biomaterials* **2017**, *147*, 68-85. (14) Chen, Z.; Liu, F.; Chen, Y.; Liu, J.; Wang, X.; Chen, A. T.; Deng, G.; Zhang, H.; Liu, J.; Hong, Z.; Zhou, J. *Adv. Funct. Mater.* **2017**, *27* (46), 1703036.
- (15) Yue, H.; Zhou, X.; Cheng, M.; Xing, D. *Nanoscale* **2018**, *10* (3), 1063-1071.
- (16) Nakamura, T.; Akita, H.; Yamada, Y.; Hatakeyama, H.; Harashima, H. *Acc. Chem. Res.* **2012**, *45* (7), 1113-1121.
- (17) Wang, P.; Zhang, L.; Zheng, W.; Cong, L.; Guo, Z.; Xie, Y.; Wang, L.; Tang, R.; Feng, Q.; Hamada, Y. *Angew. Chem.* **2018**, *57* (6), 1491-1496.

Polyethylenimine (PEI)

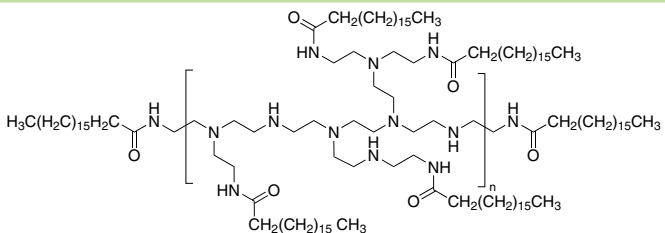
Linear PEIs

Name	Structure	Molecular Weight	Cat. No.
Polyethylenimine hydrochloride		average M_n 10,000 average M_n 4,000 average M_n 20,000	764647-1G 764892-1G 764892-5G 764965-1G
Polyethylenimine, linear		average M_n 2,500 average M_n 5,000 average M_n 10,000	764604-1G 764582-1G 765090-1G
Polyethylenimine, 80% ethoxylated solution	 R = CH ₂ CH ₂ NR ₂ R = H R = CH ₂ CH ₂ OH	M_w 110,000	306185-100G 306185-250G

Branched PEIs

Name	Structure	Molecular Weight	Cat. No.
Branched polyethylenimine solution		-	913375-5ML
Polyethylenimine, branched		average M_n ~10,000 by GPC average M_w ~25,000 by LS average M_n ~600 by GPC average M_w ~800 by LS	408727-100ML 408727-250ML 408727-1L 408719-100ML 408719-250ML 408719-1L

Modified PEIs

Name	Structure	Molecular Weight	Cat. No.
Stearic acid-modified branched polyethylenimine		-	900946-1G

Name	Structure	Molecular Weight	Cat. No.
Branched PEI-g-PEG		PEG M_n 5,000 PEG M_n 550	900743-1G 900926-1G
Acetylated branched polyethylenimine solution 20% solution		-	913235-1G

Functionalized Poly(ethylene glycol) (PEG)

Name	Structure	Molecular Weight	Cat. No.
mPEG ₁₂ -hydrazide		average M_n 650 (by NMR)	910805-500MG
mPEG ₂₄ -Hydrazide		average M_n 1200 (by NMR)	911267-500MG
mPEG ₁₂ -NHS		average M_n 700 (by NMR)	910783-500MG
mPEG ₂₄ -NHS		average M_n 1,250 (by NMR)	910813-500MG
Mal-PEG ₁₁ -Mal		average M_n 700 (by NMR)	911232-500MG
(+)-Biotin-PEG ₂₄ -Propionic acid		average M_n 1,400 (by NMR)	911194-500MG
HO-PEG ₂₄ -propanoic acid t-butyl ester		average M_n 1,200 (by NMR)	911143-500MG
Poly(ethylene glycol) bis(2-pyridyl) KAT		PEG ~10,000 Da PEG average M_n 10,000	901635-500MG

Gold Nanoparticles

Surface Group	Particle Size (nm)	λ_{max} (nm)	Cat. No.
conjugation kit	20	524 nm	900475-1EA
	40	530 nm	900477-1EA
	20	524 nm	900461-1EA
	40	530 nm	900463-1EA
Cy3 and amine functionalized	15	554 nm	905623-2.5MG
Cy3 and carboxyl functionalized	15	554 nm	905569-2.5MG
Cy3 and biotin functionalized	15	554 nm	905577-2.5MG
Cy3 and maleimide functionalized	15	554 nm	905631-2.5MG
Cy3 and methyl functionalized	15	554 nm	905658-2.5MG
Cy3 and NHS functionalized	15	554 nm	905739-2.5MG

Graphene Oxide

Name	Form	Description	Cat. No.
Graphene oxide	dispersion in H ₂ O	4 mg/mL, dispersibility: Polar solvents monolayer content (measured in 0.5mg/mL): >95%	777676-50ML 777676-200ML
	dispersion in H ₂ O	2 mg/mL	763705-25ML 763705-100ML
	dispersion (in 0.05 M HEPES buffer)	1 mg/mL, pH stabilized	901940-25ML 901940-100ML
	powder or flakes	sheets	763713-250MG 763713-1G
Graphene oxide, ammonia functionalized	dispersion in H ₂ O	1 mg/mL	791520-25ML 791520-100ML
Graphene oxide carboxylic acid enriched	dispersion in H ₂ O	2 mg/mL	795542-50ML
Graphene oxide nanocolloids	dispersion in H ₂ O	2 mg/mL	795534-50ML 795534-200ML
Sulfonated reduced graphene oxide	-	sodium salt	909130-500MG

THE FUTURE OF BIOMAGING

Nanomaterial Bioconjugation Techniques

A guide for surface modification allowing bioconjugation of inorganic nanomaterials having applications in theranostics. Discover the latest advances and protocols in nanoparticle conjugation for:

- Magnetic Imaging
- Fluorescence Imaging
- Optical-based Imaging

Order your complimentary copy from:

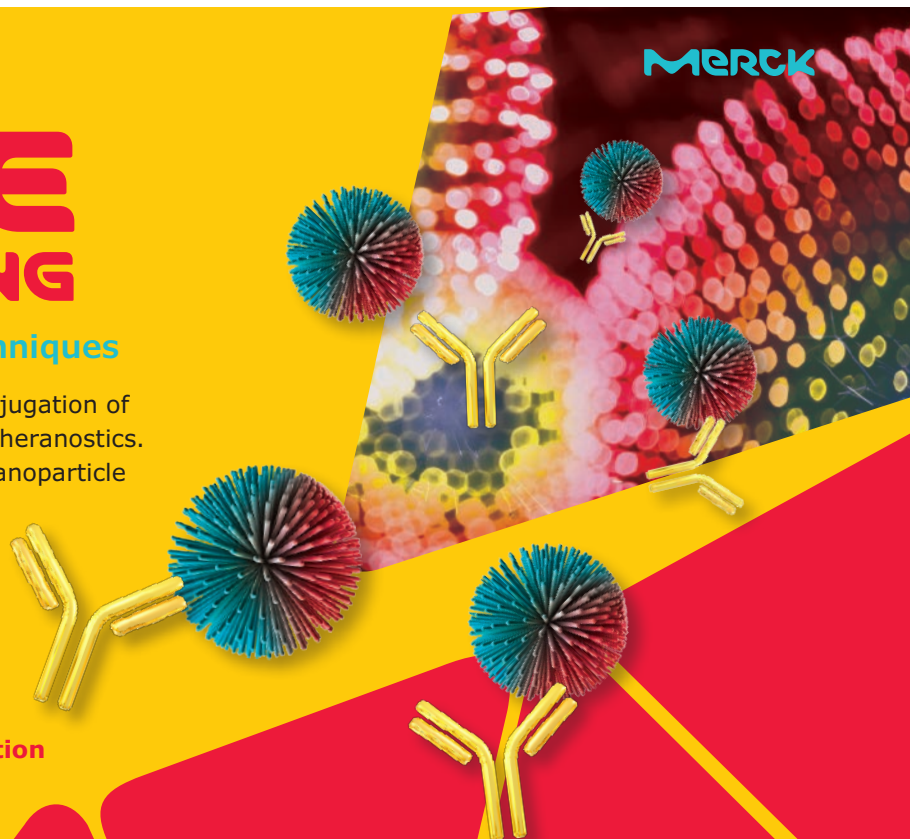
SigmaAldrich.com/nanomaterials-conjugation



The life science
business of Merck
operates as
MilliporeSigma in
the U.S. and Canada.

Sigma-Aldrich®
Lab & Production Materials

MERCK



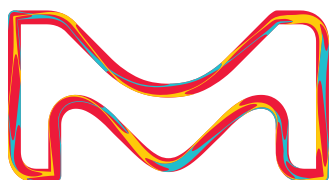
Nanomaterials for Drug Delivery and Theranostics

Enhance Your Therapeutic Efficacy and Reduce Cytotoxicity

Appropriate surface modification allows the conjugation of nanoparticles to a wide range of biomolecules, enabling their delivery and preferential accumulation at the site of action. We continue to expand our nanomaterials product portfolio, with a wide selection of nanomaterials of varying dimensions and surface functionalization for biomedical applications, including:

- Gold Nanoparticles, Nanorods, and Nanowires
- Silver nanoparticles, Nanorods, and Nanowires
- Iron Oxide Nanoparticles
- Carbon Nanotubes
- Fluorescent Nanodiamonds
- Silica Nanobeads
- Quantum Dots

To access the complete portfolio, visit SigmaAldrich.com/nanobiomed



The life science business of Merck operates as MilliporeSigma in the U.S. and Canada.

Sigma-Aldrich®
Lab & Production Materials

Smart Nanofiber Meshes as a Local Drug Delivery Platform



Mitsuhiro Ebara^{1,2,3}

¹ International Center for Materials Nanoarchitectonics (WPI-MANA), National Institute for Materials Science (NIMS), 1-1 Namiki, Tsukuba, Ibaraki 305-0044, Japan

² Graduate School of Pure and Applied Sciences, University of Tsukuba, 1-1-1 Tennodai, Tsukuba, Ibaraki 305-8577, Japan

³ Graduate School of Industrial Science and Technology, Tokyo University of Science, 6-3-1 Niiijuku, Katsushika-Ku, Tokyo 125-8585, Japan

Email: EBARA.Mitsuhiro@nims.go.jp



Introduction

Fibrous materials are playing an increasingly significant role in a variety of applications, including textiles, nonwoven substances, composite materials, and more. Polymeric nanofibers, in particular, are an exciting new class of material, attracting significant attention due to their remarkable properties, such as high specific surface area, high porosity, high molecular alignment, and nanosize effects (Figure 1A).¹ Moreover, nanofibers allow for easy incorporation of a variety of different therapeutic molecules, while expanding the drug loading capacity of the nanofibers and supporting the sustained release of embedded drug molecules (Figure 1B). Additionally, the easy manipulation of polymeric fibers as macroscopic bulk material may give rise to potential uses as implantable local drug delivery platforms.

Nanofibers can be synthesized using a variety of techniques. These include phase separation, self-assembly, electrospinning, drawing, and microfluidic methods.² One of the most widely studied techniques is electrospinning. Electrospinning offers a relatively inexpensive, straightforward method of creating a variety of continuous fibers with uniform diameters from the micro- to nanometer scale.³ It is also versatile in that almost any soluble or fusible polymer can be processed into nanofibers.

Recently, the scientific community has renewed its interest in expanding the library of available functional nanofibers different applications. Nanofibers with multi-compositions, for example, can be prepared by electrospinning polymers blended with nanoparticles, carbon nanotubes, ceramics, biomolecules, and other substances.⁴ These functional nanofibers show promise for a diverse array of applications such as tissue engineering, sensors, and wound healing. Furthermore, nanofibers with “smart” properties have attracted interest for such applications as “on-off” switchable control of permeability, wettability, and swelling/deswelling behavior.⁵ Specific polymers are used in the fabrication of smart nanofibers; these polymers are coined with

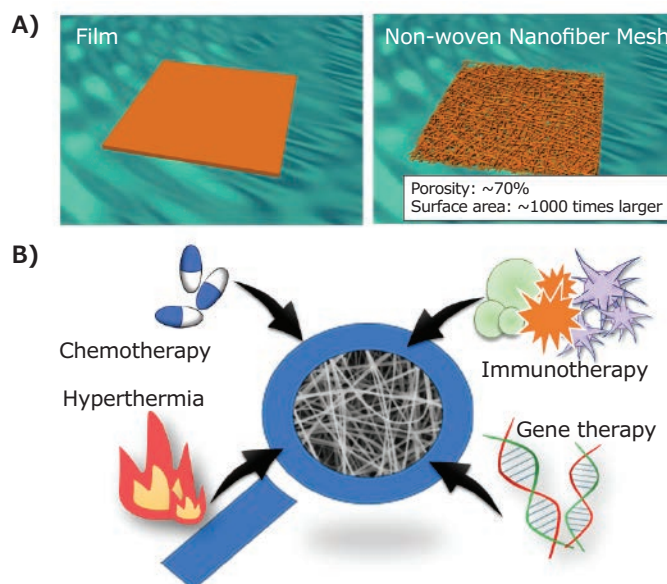


Figure 1. A) Schematic images of film and nonwoven nanofiber meshes. B) Examples of the different types of molecules that can be easily incorporated into nanofibers.

different names, based on their physical or chemical properties such as “stimuli-responsive,” “environmental-sensitive,” “smart,” or “intelligent” polymers. For consistency and clarity, the term “smart polymers” shall be used throughout the remainder of this article.

Nanofibers exhibit one characteristic that essentially defines their smartness: the ability to respond to very slight changes in the surrounding environment. The fast macroscopic changes occurring in their structure and the reversibility of these transitions demonstrate the uniqueness of these materials. Nanofibers from smart polymers can have rapid response rates

due to their inherent design features.⁶ This review focuses on the applications of smart nanofiber meshes as an implantable local drug delivery platform by introducing four types of nanofibers, as shown in **Figure 2**. These are nanofibers with sustained (type A), on-off (type B) drug release properties, and nanofibers that exist as a combination of one of these types with thermo-therapy (known as type C and D, respectively), made possible by the introduction of a heat source.

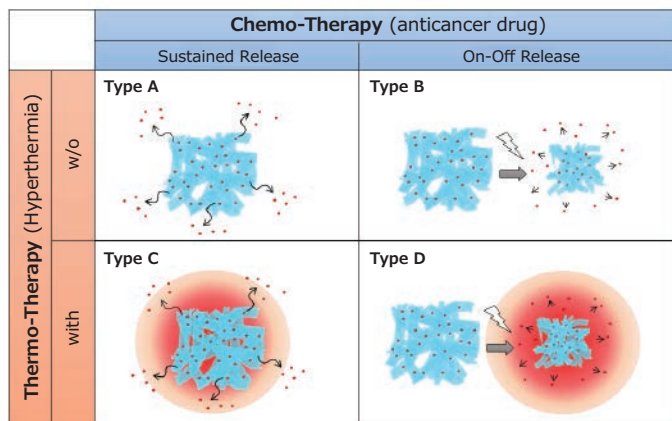


Figure 2. Four types of implantable nanofiber system for local drug delivery system proposed in this study. Nanofibers with sustained (Type A) and on-off (Type B) drug release properties combined with thermo-therapy (Type C and D, respectively).

Drug Release Control

Sustained Release (Type A)

One example of a smart material using sustained release technology is a nanofiber mesh designed for peripheral nerve injury. When a wound causes peripheral nerve damage, the patient can suffer motor paralysis, sensory paralysis, and autonomic nerve impairment. Standard treatment methods for peripheral nerve damage include directly suturing the cut or harvesting and transplanting nerves from some other part of the body. More recently, we have seen progress in the development of artificial nerves used to support nerve regeneration.

Our research group has developed a nanofiber mesh that is directly wrapped around the damaged peripheral nerves to promote regeneration and restore functionality. The nanofiber mesh is composed of poly(ϵ -caprolactone) (PCL), a biodegradable aliphatic polyester approved by the US Food and Drug Administration (FDA) for biomedical applications such as drug delivery, tissue engineering scaffolds, and implant materials.⁷ Scientists synthesized PCL by ring-opening polymerization from terminal hydroxyl groups of an initiator using tin octoate (Cat. No. **S3252**) as catalyst.⁸ PCL nanofibers were produced by an electrospinning method using 1,1,1,3,3,3-hexafluoroisopropanol (HFIP, Cat. No. **105228**) as a solvent.

The mesh contains methylcobalamin (MeCbl), an active vitamin B12 homolog delivered favorably to nerve tissues, proving effective in promoting nerve regeneration and neuronal cell survival. PCL nanofiber meshes gradually released MeCbl

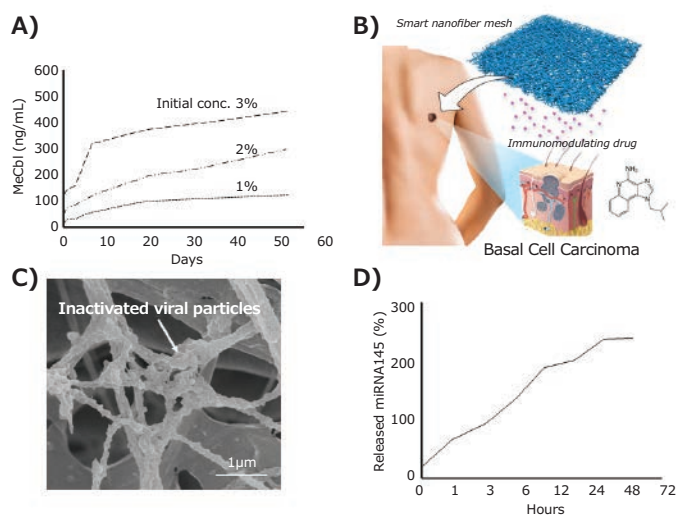


Figure 3. A) Drug release behavior of methylcobalamin (MeCbl) from PCL nanofiber meshes. B) Schematic image of immunomodulating drug-incorporated nanofiber mesh for basal cell carcinoma therapy. C) Scanning electron microscopic image of inactivated viral particles-modified PCL nanofiber mesh for prostate cancer therapy. D) Drug release behavior of micro RNA 145 from PCL nanofiber mesh.

for at least 8 weeks when tested in vitro (**Figure 3A**).

Local implantation of nanofiber sheets incorporating MeCbl successfully contributed to the recovery of motor and sensory function, the recovery of nerve conduction velocity, and the promotion of myelination after sciatic nerve injury, without affecting plasma concentration of MeCbl.⁹

We have also tested the PCL nanofiber systems with an immune-modulating agent (**Figure 3B**),¹⁰ inactivated virus (**Figure 3C**),¹¹ and microRNA (**Figure 3D**) for the treatment of basal cell carcinoma, prostate cancer cells, and liver cancer cells, respectively. These examples suggest the advantages of nanofiber systems in which different types of molecules can be easily incorporated regardless of molecular size, shape, surface charge, and hydrophilicity.

On-off Switchable Release (Type B)

In addition to sustained release, temporal control of drug administration is critical for effective chemotherapy. Recently, a new medication concept called “dose-dense chemotherapy” has gained much attention, as it achieves maximum tumor destruction by increasing the rate of chemotherapy delivery, rather than by increasing dosage. Administration of a weekly dose of chemotherapy, rather than every 3 weeks, allows the treatment to interrupt the rapid growth phase of the tumor cells.¹³

Given this situation, smart nanofiber meshes have the potential to be used for temporal drug release triggered by external stimuli. However, one of the significant challenges in the development of smart nanofiber meshes is the design of nanofibers with dynamically and reversibly tunable fiber structures on both the nano- and macro-scopic scale. This was achieved by electrospun copolymers of *N*-isopropylacrylamide (NIPAAm, Cat. No. **731129**) with a UV-reactive benzophenone (BP) conjugated co-monomer.¹⁴ These photo-crosslinkable,

temperature-responsive, polymer-based nanofiber meshes demonstrated dynamically and reversibly tunable properties, including swelling/shrinking, mechanical strength, and porosity. However, one shortcoming of this method is that the phase transition temperature of the copolymer decreases after the conjugation because of the hydrophobic nature of BP. Therefore, we also fabricated smart nanofibers by electrospinning copolymers of NIPAAm and *N*-hydroxymethyl acrylamide (HMAAm) because the hydroxyl groups of HMAAm are subsequently crosslinked by thermal curing. The successful fabrication of copolymers into a well-defined nanofibrous structure with a diameter of about 600–700 nm, where the fibers preserved their morphology even after thermal curing.

The resulting crosslinked nanofibers showed rapid and reversible volume changes in aqueous media in response to cycles of temperature alternation around body temperature.¹⁵ The on-off switchable release of dextran from the crosslinked nanofibers was observed. Almost all the dextran was released from the nanofibers after six heating cycles, whereas only a negligible amount of dextran was evolved during the cooling process. These drug release profiles, show that the proposed system can

release a certain amount of a drug in response to the circadian rhythm of the disease. This allows for the use of such a system for the optimal treatment of chronic diseases that show circadian variation such as asthma, hypertension, myocardial infarction, and arthritis.

Combination with Hyperthermia

Sustained Release with Heat (Type C)

Although chemotherapy has historically been the standard treatment for primary and metastatic cancer, its clinical benefits are still limited when administering a single anticancer drug. Therefore, combination chemotherapy regimens containing two or more classical anticancer drugs have been applied in clinical practice to treat a variety of cancers in the past decades. For example, numerous clinical trials have shown a significant reduction in tumor size when combining chemotherapy with other treatments such as radiotherapy and thermal therapy.¹⁶ Thermal therapy, also called hyperthermia, is a type of cancer treatment in which body tissue is exposed to high temperatures (43–45 °C).

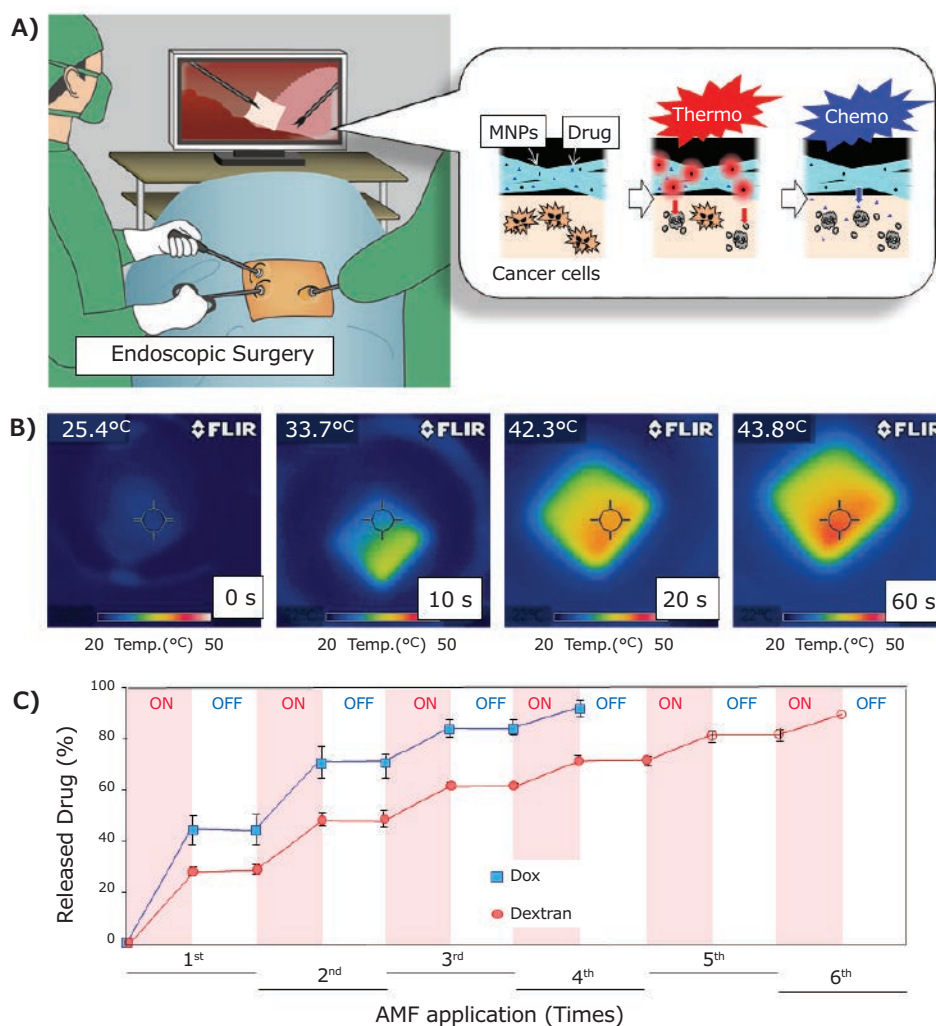


Figure 4. A) Schematic illustration for on-off switchable temperature-responsive fiber mesh for cancer thermo-chemotherapy. B) The infrared thermal images of MNPs-loaded nanofiber mesh in AMF. C) On-off switchable drug release profiles for DOX and dextran from temperature-responsive nanofiber meshes in response to AMF application.

Hyperthermia can also enhance the effects of certain anticancer drugs such as paclitaxel (PTX), making some cancer cells more sensitive to treatment. From these perspectives, we have designed a smart nanofiber system using a combination of chemotherapy and hyperthermia for more effective cancer therapy (**Figure 4A**).¹⁷ The mesh is composed of biodegradable PCL with PTX and magnetic nanoparticles (MNPs) (**Figure 4B**). The PCL mesh released PTX slowly for at least 6 weeks when tested *in vitro*. The prolonged therapeutic effect observed *in vivo* as a continuous release of medication from the mesh over an extended period compared with the direct injection of PTX into the tumor site. Also, the synergistic anticancer effect was achieved upon excitation of the mesh with an alternating magnetic field (AMF) because the MNPs within the nanofiber generated localized heat, which caused heat-induced cell killing as well as enhanced chemotherapeutic effect of PTX.

Based on these results, the smart nanofiber system shows promise for cancer therapeutics in the future and may provide new insights for the future development of localized thermo/chemotherapy.

On-off Switchable Release with Heat (Type D)

On-off switchable drug delivery systems have also gained attention from the viewpoints of circadian clocks.¹⁸ For example, programmable-in-time drug delivery systems are being used as chronotherapeutics. Combining this system with hyperthermia treatments promotes PTX-induced apoptosis through the activation of caspase-7, increasing the proportion of cells arrested in G2/M, thereby reducing the IC₅₀ of PTX.

Given these backgrounds, we have been developing a smart hyperthermia nanofiber system with simultaneous heat generation and drug release in response to on-off switching of AMF for the induction of cancer apoptosis.¹⁹ The nanofiber is composed of a chemically-crosslinkable temperature-responsive polymer, poly(NIPAAm-co-HMAAm) with an anticancer drug (doxorubicin; DOX) and MNPs. An electrospinning method was employed to fabricate the mesh.

By chemical crosslinking, the nanofiber mesh exhibits switchable changes in the swelling ratio in response to alternating on-off switches of AMF because the self-generated heat from the incorporated MNPs induces the deswelling of polymer networks in the nanofiber, allowing the observation of the corresponding on-off release of DOX from the nanofibers in response to AMF (**Figure 4C**). 70% of human melanoma cells died in a 5 min application of AMF in the presence of MNPs and DOX incorporated nanofibers through the double effect of heat and drug.

This smart hyperthermia has also been applied to lung adenocarcinoma. The phase transition temperature of the temperature-responsive mesh was adjusted to the mild-hyperthermia temperature range of around 43 °C. *In vitro*

anti-tumor studies demonstrated that both MNP- and PTX-loaded mesh killed about 66% of cells, whereas mesh loaded with only PTX killed about 43% of cells.²⁰ In a mouse lung cancer model, the thermo-chemotherapy combo displayed enhanced anti-tumor activity, eliminating the systemic toxic effects on the mice due to local release of the chemotherapeutic agents. We believe that these types of proposed fiber system may provide a blueprint to guide the design of the next generation of local drug delivery systems for safe and effective cancer treatment.

Conclusions

Fibers of various types at various production stages have already been explored for a wide range of applications in diverse fields, including nanotechnology, textiles, industry, fuel cells, tissue engineering, regenerative medicine, and biomaterials. These fibers, particularly well-defined nanofibers, have astounding features compared with other types of materials. For instance, high specific surface area, high porosity, and biomimetic properties provide promising potential applications.

Among these fibers, those that can be combined with stimuli-responsive media are known as smart fibers. Smart fibers can be controlled remotely by applying external stimuli, without changing other fiber characteristics. The dynamic nature of these smart fibers can also be used to induce mechanical forces that lead to changes in cellular behavior.²¹ Taking all the merits of smart fibers into account, these materials can be utilized as tools for a wide range of applications.

Acknowledgment

The author would like to acknowledge financial support by JSPS KAKENHI (Grant Number 264086 and 26750152). The author is grateful to Prof. Allan S. Hoffman (University of Washington) for continued and valuable comments and discussion.

References

- (1) Niiyama, E. et al. *Smart Textiles: Wearable Nanotechnology*. Ed. N. D. Yilmaz, Wiley, **2018**, 111.
- (2) Kim, Y. et al. *Smart Biomaterials*. NIMS Monographs. Springer, **2015**, 189.
- (3) Namekawa, K. et al. *Biomaterials Sci.* **2014**, *2*, 674.
- (4) Takai, R. et al. *J. Nanomater.* **2016**, *2016*, 5638905.
- (5) Bou, S. et al. *Curr. Opin. Biotech.* **2016**, *39*, 113.
- (6) Maeda, T. et al. *Fibers* **2017**, *5*, 13.
- (7) Uto, K. et al. *Sci. Technol. Adv. Mater.* **2012**, *13*, 064207.
- (8) Ebara, M. et al. *Adv. Mater.* **2012**, *24*, 273.
- (9) Suzuki, K. et al. *Acta Biomater.* **2017**, *53*, 250.
- (10) Garrett, R. et al. *Fibers* **2015**, *3*, 478.
- (11) Okada, T. et al. *Biomaterials Sci.* **2016**, *4*, 96.
- (12) Che, H.L. et al. *J. Nanosci. Nanotech.* **2015**, *15*, 7971.
- (13) Katsumata, N. et al. *Lancet Oncol.* **2013**, *14*, 1020.
- (14) Kim, Y. et al. *Adv. Funct. Mater.* **2013**, *23*, 5753.
- (15) Kim, Y. et al. *Sci. Technol. Adv. Mater.* **2012**, *13*, 064203.
- (16) Urano, M. et al. *Int. J. Hyperthermia* **1999**, *15*, 79.
- (17) Niiyama, E. et al. *Adv. Health. Mater.* **2019**, *34* (3), 179.
- (18) Lévi, F. et al. *Expert Opin. Drug Del.* **2011**, *8*, 1535.
- (19) Kim, Y. et al. *Angew. Chem. Intl. Ed.* **2012**, *51*, 10537.
- (20) Niiyama, E. et al. *Polymers* **2018**, *10*, 1018.
- (21) Mano, S.S. et al. *Theranostics* **2017**, *7*, 4658.

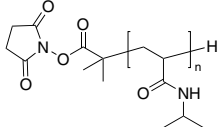
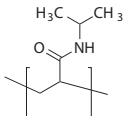
Biodegradable Polymers

Poly(caprolactone)

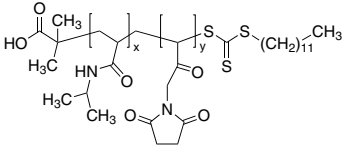
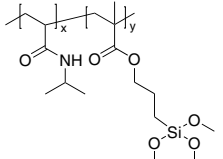
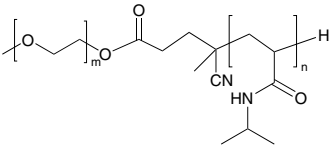
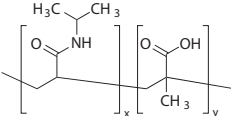
Name	(dL/g)	Cat. No.
Resomer® C 209, Poly(caprolactone)	viscosity 0.8-1.0	769762-5G 769762-25G
Resomer® C 212, Poly(caprolactone)	viscosity 1.13-1.38	769754-5G 769754-25G
Polycaprolactone	viscosity 2.2	900288-5G
	viscosity 1.5	900297-5G
	viscosity 2.7	900296-5G
	viscosity 0.40	900825-5G
	viscosity 0.20	900824-5G
	viscosity 1.2	900822-5G
	viscosity 1.7	900820-5G

Responsive Polymers

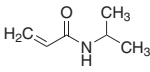
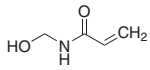
Poly(*N*-isopropylacrylamide)

Name	Structure	Molecular Weight	Cat. No.
Poly(<i>N</i> -isopropyl acrylamide)		average M_n 5,000	900188-1G
Poly(<i>N</i> -isopropylacrylamide)		M_n 20,000-60,000	535311-10G
		average M_n 30,000	806471-1G
		M_n 60,000-110,000	901422-10G

Poly(*N*-isopropylacrylamide) Copolymers

Name	Structure	Molecular Weight	Cat. No.
Poly(<i>N</i> -isopropyl acrylamide- <i>co</i> -(<i>N</i> -methacryloxysuccinimide))		average M_n 5,000	809489-1G
Poly(<i>N</i> -isopropyl acrylamide- <i>co</i> -3-(trimethoxysilyl)propyl methacrylate)		average M_n 10000	900189-1G 900189-5G
Poly(ethylene glycol)- <i>block</i> -poly(<i>N</i> -isopropylacrylamide)		PEG M_n 2,000 PNIPAM M_n 24,000	747181-500MG
Poly(<i>N</i> -isopropylacrylamide- <i>co</i> -methacrylic acid)		average M_n 50,000 M_n 60,000	724467-5G 724858-5G

Monomers

Name	Structure	Purity	Cat. No.
N-Isopropylacrylamide		97%	415324-10G
		≥99%	415324-50G
N-(Hydroxymethyl)acrylamide solution		-	731129-5G
			731129-25G
			245801-100G
			245801-1KG

Magnetic Nanoparticles

Name	Average Particle Size	Purity & Concentration	Form	Cat. No.
Iron oxide(II,III), magnetic nanoparticles solution	5 nm	5 mg/mL in H ₂ O	dispersion	725331-5ML
	10 nm	5 mg/mL in H ₂ O	dispersion	725358-5ML
	10 nm	Fe 5 mg/mL in H ₂ O	dispersion	747254-2ML
	20 nm	5 mg/mL in H ₂ O	dispersion	725366-5ML
	30 nm	Fe 1 mg/mL in H ₂ O	dispersion	747327-10ML
	10 nm	Fe 1 mg/mL in H ₂ O	dispersion	747424-1ML
	5 nm	Fe 1 mg/mL in H ₂ O	dispersion	747343-10ML
	10 nm	Fe 1 mg/mL in H ₂ O	dispersion	747319-10ML
	10 nm	Fe 1 mg/mL in H ₂ O	dispersion	747300-10ML
	30 nm	Fe 1 mg/mL in H ₂ O	dispersion	747408-10ML
	5 nm	Fe 1 mg/mL in H ₂ O	dispersion	747416-1ML
	5 nm	Fe 1 mg/mL in H ₂ O	dispersion	790508-10ML

be sciencesational

MERCK

Bolder chemistry to empower your discovery

Scientific discovery is a revolution, not an evolution. It requires products you know and trust. But also, some you've never seen before.

Discover how we help you to stay sciencesational on: SigmaAldrich.com/sciencesational



The life science business of Merck operates as MilliporeSigma in the U.S. and Canada.

Sigma-Aldrich[®]
Lab & Production Materials

The Potential of Dendritic Polyester Scaffolds as Biocompatible Drug Delivery Agents

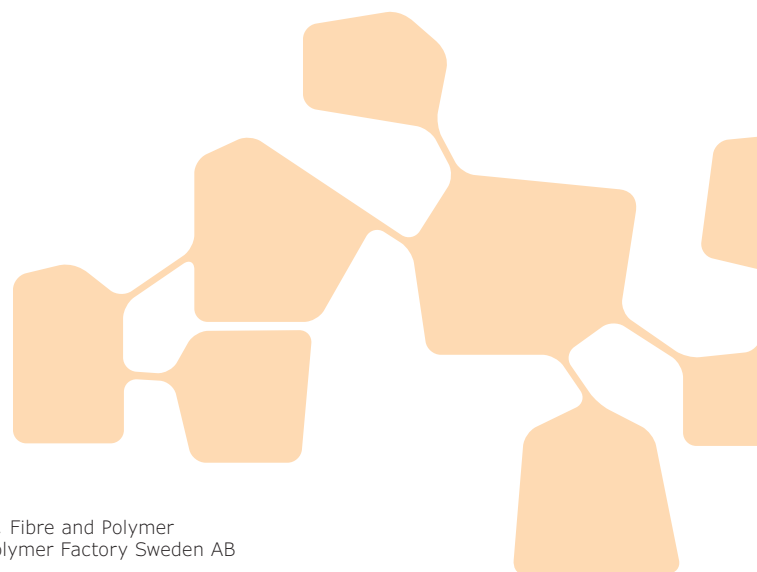


Dr. Jamie Godfrey¹ and Dr. Michael Malkoch^{2*}

¹ Product Manager, Polymer Factory Sweden AB.

² Professor of Functional Organic Nanomaterials, Division of Coating Technology, Fibre and Polymer Technology, KTH Royal Institute of Technology, and Chief Executive Officer, Polymer Factory Sweden AB

* Email: michael.malkoch@polymerfactory.com



Introduction/Background

Dendrimers, dendrons and linear dendritic hybrids comprise a family of synthetic macromolecules containing a large number of branches, and thus a multitude of peripheral groups. These molecules are constructed in a layer-by-layer fashion, in which each layer is termed a generation. Due to the high degree of control afforded by this approach, and in contrast to the broader family of hyperbranched polymers, true dendrimers exhibit practically defect-free architectures, and provide unrivaled control over molecular weight, number of peripheral functional groups and nanoscale size, resulting in unparalleled batch-to-batch consistency. These unique properties have made dendritic polymers attractive candidates for biomedical applications, particularly in the design of drug delivery systems, imaging probes, and the introduction of targeting moieties. As such, dendrimers and dendrons display several advantages over their less well-defined counterparts, including:

- large and exact payload of drug molecules for targeting motifs or other bioactive units due to large and precise number of peripheral groups
- predictable and reproducible structure activity relationships due to batch-to-batch consistency and lack of defects
- inherently modular and customizable structures, both from the ground up and at the periphery, allowing tuning of water solubility and degradation in physiological conditions.

- encapsulation of hydrophobic or hydrophilic drugs as a passive delivery system based on a well-defined interior
- ability to combine multiple modes of action in the same carrier, e.g., bifunctional nano-carriers loaded with both drug and imaging probes for visualization of delivery

Types of Dendrimers

Vögtle et al.,¹ Newkome et al.,² and Tomalia et al.,³ pioneered the synthesis of dendrimers, with Tomalia's contribution leading to the poly(amidoamine), or PAMAM, dendrimers becoming the first commercially available family of dendrimers. PAMAM dendrimer construction occurs via the formation of subsequent amine and amide linkages, with the final macromolecule displaying amino surface groups at the periphery.

PAMAM dendrimers show considerable cytotoxicity to several cell lines,⁴⁻⁶ with their biocompatibility compromised by a relatively hydrolytically stable interior, preventing timely degradation in the body. Additionally, unavoidable side reactions during synthesis often lead to the presence of structural defects, reducing the dendritic purity and precise nature of the molecules. For example, a fourth-generation PAMAM dendrimer may contain only 8% defect-free product.⁷

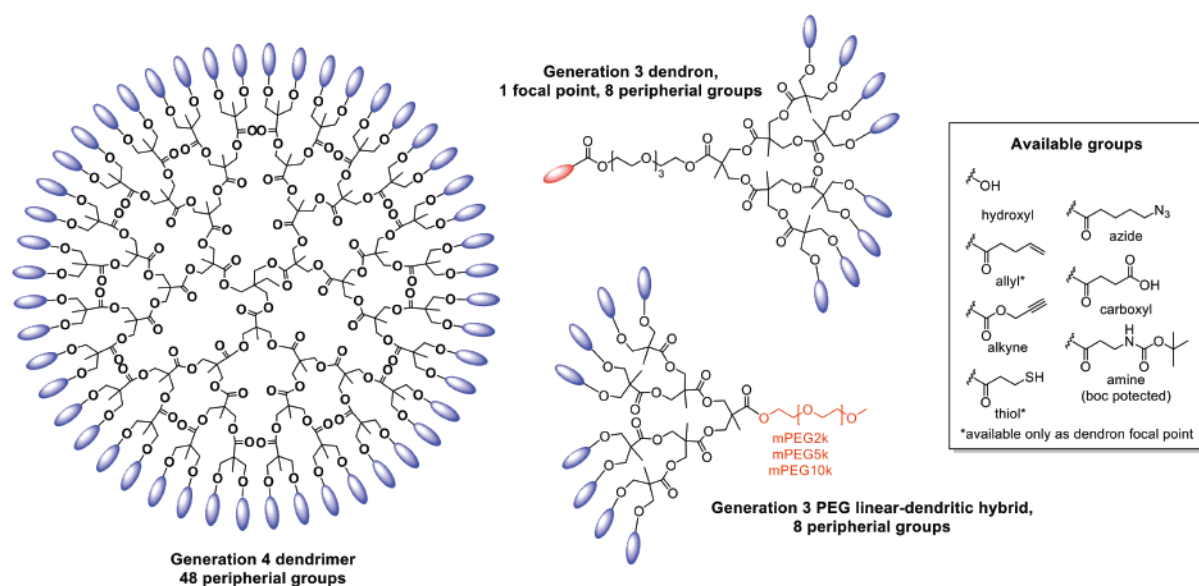


Figure 1. Examples of functional bis-MPA based dendritic structures commercially available through Merck.

Hult et al. introduced a class of dendrimers with a polyester scaffold in 1996,⁸ which have since produced an extensive library of multifunctional dendrimers, dendrons, and linear dendritic hybrid block copolymers (Figure 1), many of which are commercially available through Merck and Polymer Factory. In contrast to other widely used dendrimers, the family of bis-MPA dendrimers presents low or no *in vitro* toxicity, no specific *in vivo* organ accumulation, no immunogenic profile, and are biodegradable under physiological conditions.^{4,5} Other characteristics that make these molecules attractive for biomedical applications and drug delivery systems include the availability of a range of architectures (e.g., dendrons that present two orthogonal functionalities as linkers and signal amplifiers for molecules of interest), as well as the availability of scaffolds that possess a range of reactive groups for simple modification with a drug or bioactive substrates. The structural perfection attainable with bis-MPA based dendrimers has been further highlighted by their use as mass spectrometry calibration standards, with no structural defects detected even up to the fifth generation.⁹ Herein, a highlight of the drug delivery and related applications realized using bis-MPA dendritic materials is presented.

Bis-MPA Dendritic Scaffolds for Drug Delivery and Targeting

The majority of polymeric drug delivery systems (DDS) can be separated into two categories: passive strategies where the drug is physically entrapped in the interior of a delivery vessel via hydrophobic or ionic interactions, and covalent attachment of drug molecules directly to the polymeric scaffold.

Delivery via Passive Entrapment

Passive encapsulation strategies using dendritic polymers have primarily been based on one of two approaches: (1) formation of micelles and other nanostructures with amphiphiles based on

bis-MPA linear-dendritic block copolymers, or (2) modification of dendritic structures with a hydrophilic corona, allowing water solubility while maintaining a hydrophobic interior for loading of non-polar cargo such as drug molecules.

The groups of Nyström and Malkoch evaluated both poly(ethylene glycol) (PEG) linear-dendritic hybrids and their less well defined hyperbranched analogs as micellar carriers of anti-cancer drugs.¹⁰ The authors observed that the carriers before drug loading showed no dose-dependent toxicity toward the cancer cell lines tested, while the therapeutically loaded micelles increased the efficacy vs the free drug. Subsequently, Malkoch, Hawker et al. expanded on this work, utilizing the bifunctional nature of PEG bis-MPA linear-dendritic hybrids to construct fluorescent-tagged, supramolecular self-assemblies of nanoscale size.¹¹ The nano-carriers were loaded with nearly 20 wt % of doxorubicin (DOX) and triptolide (TPL), increasing the therapeutic efficacy for both drugs, as well as their combinations, against human breast cancer cell lines. Additionally, the fluorescent tag afforded by the precision nature of the linear dendritic structure allowed intracellular tracking of the nano-carrier, elucidating the mechanism of improved action at a cellular level. Frechet et al. also used PEG linear dendritic hybrids to form DOX loaded micelles with acetal groups at the hydrophobic termini, allowing disruption of the micelles and triggering release under mildly acidic condition.¹² These pH-responsive nano-carriers were designed for the controlled release of the chemotherapeutic agent at the elevated pH of tumor sites.

Malmström, Nyström, et al. demonstrated an alternative approach, whereby the formation of core-shell nanoparticles occurred spontaneously by controlled radical polymerization of oligo(ethylene glycol) methacrylate monomer from multifunctional dendritic initiators.¹³ Through the incorporation of fluorinated co-monomer, dual functional theranostic nanoparticles were obtained, capable of passive loading with

DOX and other hydrophobic drugs, as well as imaging via ^{19}F -MRI. The authors observed controllable drug release kinetics noted the possibility to tune the release profile through variation of the dendritic hydrophobic segment.

PAMAM and poly(propylene imine) (PPI) dendrimers have emerged as promising candidates as non-viral gene delivery vectors in gene therapy. The polycationic nature of these macromolecules allows them to bind to nucleic acids at physiological pH.¹⁴ However, PAMAM and PPI dendrimers are highly stable in physiological solution, preventing degradation of the carrier and preventing safe clearance from the body.⁵ Malkoch et al. recently reported that bis-MPA dendrimers could be modified with *beta*-alanine peripheral groups, providing a polycationic macromolecular structure, analogous to those of PAMAM, while maintaining a polyester interior capable of rapid degradation under biologically relevant conditions.¹⁵ The amine functional polyester dendrimers displayed an increase in neurotoxicity compared to the neutral bis-MPA scaffolds, but a lower neurotoxicity than commercially available PAMAM dendrimers. These molecules were further evaluated as non-viral vectors for siRNA delivery:¹⁶ G2 to G4 dendrimers bearing 12 to 48 amino end-groups were capable of siRNA complexation and subsequent protection of siRNA from degradation by RNase, leading to a 20% decrease of target protein expression.

Delivery via Covalent Attachment

Due to the hydrophobic nature of many pharmaceutically active compounds, covalent attachment to biocompatible polymeric scaffolds is an attractive method for increasing aqueous solubility, introducing active or passive targeting for desired cells/tissues and tuning of the release profile. Dendritic frameworks based on bis-MPA are versatile structures for covalent attachment of drug molecules: they are commercially available with a range of reactive groups easily manipulated via efficient chemistries, possess several peripheral groups for

increased payloads or additional targeting/imaging moieties, and also can include orthogonal reactive groups for dual functional delivery systems. The range of available methods for drug attachment also allows for the tailoring of the linking chemistry to further control the release of active drugs through external stimuli, such as pH or the reductive potential of a cell.

The dual-functionality possible with bis-MPA scaffolds was exploited by Fréchet et al. to construct “bow-tie” bifunctional dendrimers with pH-sensitive linkages at one face, and multiple PEG chains at the other to provide aqueous solubility and optimized blood circulation time.¹⁷ This dendrimer DDS gave a nine-fold increase in specific tumor uptake compared to a free drug in a colorectal animal model. Sharpless, Hawker et al. utilized a similar approach of bifunctional dendrimer design, to produce dendrimers containing exact numbers of mannose units for recognition/targeting, along with coumarin for detection through fluorescence (Figure 2).¹⁸ The dendrimers showed a 240-fold increased potency for the inhibition of hemagglutination. A critical advantage of coupling functional dendrons to give dual-functional “bow-tie” dendrimers lies in the absolute control that can be achieved through a modular synthesis. High batch-to-batch consistency can be achieved with good optimization of linking chemistry, allowing carriers with exact numbers of each functional moiety; this is in stark contrast to methods of adding multifunctional units to a pre-existing carrier in a statistical manner, which unavoidably leads to an undefined mixture unlikely pass regulatory revision and translate to the clinic.¹⁹

Bifunctional dendrons based on bis-MPA have great potential for the linking of drugs, diagnostic probes, or bioactive molecules to tailor or improve their properties. Their bifunctional nature allows simple covalent attachment of molecules of interest at the core, with orthogonal peripheral groups providing a broad and exact number of further chemical handles to tailor solubility or other desired properties further. Valliant, Adronov et al. introduced

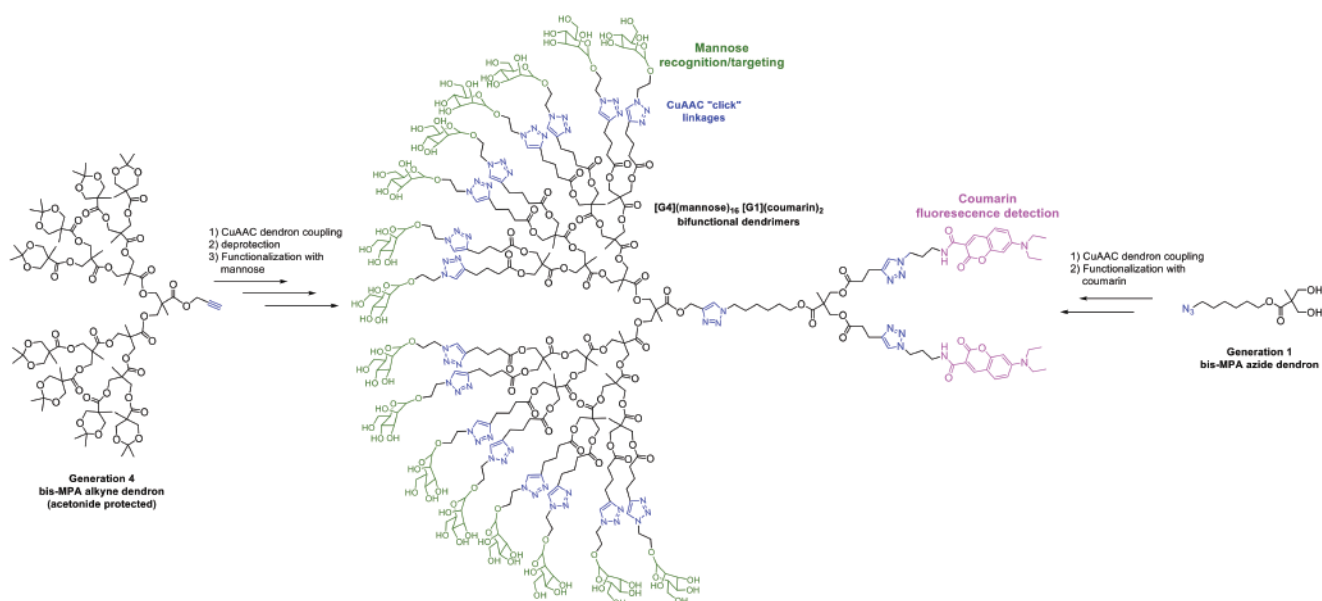


Figure 2. Synthetic scheme showing the construction of bifunctional dual-purpose recognition/detection dendrimers. Adapted with permission from reference 18, copyright 2005 Royal Society of Chemistry.

a tridentate ligand capable of forming stable complexes with ^{99m}Tc to bis-MPA dendrons of generations 4 through 7, creating radiolabeling probes.²⁰ The subsequent *in vivo* SPECT imaging revealed that the dendrimers were cleared from the body of the rats within 15 minutes, with no retention in any organ. The authors noted that the study enables further investigation of targeting via surface functionalization in further studies. Ellis-Davies et al. utilized a similar strategy to introduce water solubility and avoid unwanted GABA receptor antagonism of chemical probes for two-photo optoneurobiology.²¹ The authors conjugated generation 4 and 5, alkyne focal point dendrons to a series of probes via CuAAC “click” chemistry, allowing for the study of the signaling of GABA in its natural state for the first time. Another example of the attachment of imaging probes to a dendritic scaffold, has been demonstrated by the attachment of fluorescent dyes to the periphery of bis-MPA dendrons allowing dual-functional therapeutics with imaging capability.²² The authors introduced multiple, exact numbers of Cy5 dye to the surface of generation 1 to 3 dendrons, and showed that generation 3 dendrons amplified the fluorescent signal vs the lower generation dendrons and a monofunctional control. A chemoselective focal point was retained in the molecules, allowing labelling of an antibody without jeopardizing activity.

Functionalization Strategies for Commercially Available bis-MPA Dendrons

The wide range of commercially available polyester dendrimer and dendrons allows the development of new macromolecules tailored to specific drug delivery targets. These can be fabricated by exploiting several efficient and straightforward chemical modifications, ideally operating in an orthogonal manner and avoiding the use of protecting chemistry. Development of conjugation chemistries over the past two decades based on “click” chemistry principles,²³ are presented in **Table 1**. Such chemistries have been used for the conjugation of a diverse range of biologically active substrates to bis-MPA scaffolds, including PEG,^{10,24} sugar units,¹⁸ drug molecules,¹⁷ biotin,²⁵ and fluorescent probes.²²

Summary

Dendrimers, dendrons, and linear-dendritic hybrids are among the most sophisticated materials available to scientists aiming to deliver and enhance the effect of biologically active molecules. Due to their precise and modular nature, along with a range of efficient conjugation chemistries, countless iterations of advanced DDS frameworks are now possible. The commercial availability of these structures may provide non-specialist chemists the toolbox to build the next generation of drug delivery systems.

References

- (1) Buhleier, E.; Wehner, W.; Vögtle, F. *Synthesis (Stuttg)*. **1978**, 1978 (02), 155158.
- (2) Newkome, G. R.; Yao, Z.; Baker, G. R.; Gupta, V. K. *J. Org. Chem.* **1985**, 50 (11), 2003–2004.
- (3) Tomalia, D. A.; Baker, H.; Dewald, J.; Hall, M.; Kallos, G.; Martin, S.; Roeck, J.; Ryder, J.; Smith, P. *Polym. J.* **1985**, 17 (1), 117–132.
- (4) Movellan, J.; González-Pastor, R.; Martín-Duque, P.; Sierra, T.; de la Fuente, J. M.; Serrano, J. L. *Macromol. Biosci.* **2015**, 15 (5), 657–667.

Table 1. Common coupling reactions for functional groups of commercially available dendritic functional groups, with references utilizing similar procedures.

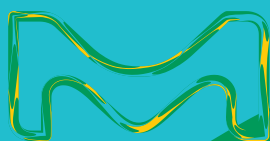
Dendritic functional group	Reactive toward	Coupling Reaction (ref)
Allyl	Thiol	Thiol-ene ^{24,26,27}
Alkyne	Thiol Azide	Thiol-yne ²⁶ CuAAC ¹⁸
Thiol	Alkenes/alkynes	Thiol-ene Thiol-yne
Azide	Alkyne	CuAAC
Primary amine (NHBoc protected)	NHS-ester Carboxyl	NHS amidification ¹⁵ EDC/DDC amidation
Carboxyl	Amines Hydroxyl	EDC/DDC amidation Fluoride promoted esterification ^{25,28}
Hydroxyl	Carboxyl	Fluoride promoted esterification

- (5) Feliu, N.; Walter, M. V.; Montañez, M. I.; Kunzmann, A.; Hult, A.; Nyström, A.; Malkoch, M.; Fadeel, B. *Biomaterials* **2012**, 33 (7), 1970–1981.
- (6) Feliu, N.; Kohonen, P.; Ji, J.; Zhang, Y.; Karlsson, H. L.; Palmberg, L.; Nyström, A.; Fadeel, B. *ACS Nano* **2015**, 9 (1), 146–163.
- (7) Mintzer, M. A.; Grinstaff, M. W. *Chem. Soc. Rev.* **2011**, 40 (1), 173–190.
- (8) Ihre, H.; Hult, A.; Söderlind, E. *J. Am. Chem. Soc.* **1996**, 118 (27), 6388–6395.
- (9) Grayson, S. M.; Myers, B. K.; Bengtsson, J.; Malkoch, M. *J. Am. Soc. Mass Spectrom.* **2014**, 25 (3), 303–309.
- (10) Hed, Y.; Zhang, Y.; Andrén, O. C. J.; Zeng, X.; Nyström, A. M.; Malkoch, M. *J. Polym. Sci. Part A Polym. Chem.* **2013**, 51 (19), 3992–3996.
- (11) Andrén, O. C. J.; Zhang, Y.; Lundberg, P.; Hawker, C. J.; Nyström, A. M.; Malkoch, M. *Chem. Mater.* **2017**, 29 (9), 3891–3898.
- (12) Gillies, E. R.; Fréchet, J. M. J. *Bioconjug. Chem.* **2005**, 16 (2), 361–368.
- (13) Porsch, C.; Zhang, Y.; Östlund, Å.; Damberg, P.; Ducani, C.; Malmström, E.; Nyström, A. M. *Part. Part. Syst. Charact.* **2013**, 30 (4), 381–390.
- (14) de Araújo, R. V.; da Silva Santos, S.; Ferreira, E. I.; Giarolla, J. *Molecules* **2018**, 23 (11), 1–27.
- (15) Stenström, P.; Hjorth, E.; Zhang, Y.; Andrén, O. C. J.; Guette-Marquet, S.; Schultzberg, M.; Malkoch, M. *Biomacromolecules* **2017**, 18 (12), 4323–4330.
- (16) Stenström, P.; Manzanera, D.; Zhang, Y.; Ceña, V.; Malkoch, M. *Molecules* **2018**, 23 (8), 2028.
- (17) Lee, C. C.; Gillies, E. R.; Fox, M. E.; Guillaudeu, S. J.; Fréchet, J. M. J.; Dy, E. E.; Szoka, F. C. *Proc. Natl. Acad. Sci.* **2006**, 103 (45), 16649–16654.
- (18) Wu, P.; Malkoch, M.; Hunt, J. N.; Vestberg, R.; Kaltgrad, E.; Finn, M. G.; Fokin, V. V.; Sharpless, K. B.; Hawker, C. J. *Chem. Commun.* **2005**, 46, 5775–5777.
- (19) Goonewardena, S. N.; Kratz, J. D.; Zong, H.; Desai, A. M.; Tang, S.; Emery, S.; Baker, J. R.; Huang, B. *Bioorg. Med. Chem. Lett.* **2013**, 23 (10), 2872–2875.
- (20) Parrott, M. C.; Benhabbour, S. R.; Saab, C.; Lemon, J. A.; Parker, S.; Valliant, J. F.; Adronov, A. *J. Am. Chem. Soc.* **2009**, 131 (8), 2906–2916.
- (21) Richers, M. T.; Amatrudo, J. M.; Olson, J. P.; Ellis-Davies, G. C. R. *Angew. Chemie* **2017**, 129 (1), 199–203.
- (22) Martín-Serrano Ortiz, Á.; Stenström, P.; Mesa Antunez, P.; Andrén, O. C. J.; Torres, M. J.; Montañez, M. I.; Malkoch, M. *J. Polym. Sci. Part A Polym. Chem.* **2018**, 56 (15), 1609–1616.
- (23) Kolb, H. C.; Finn, M. G.; Sharpless, K. B. *Angew. Chemie Int. Ed.* **2001**, 40 (11), 2004–2021.
- (24) Conte, M. Lo; Robb, M. J.; Hed, Y.; Marra, A.; Malkoch, M.; Hawker, C. J.; Dondoni, A. *J. Polym. Sci. Part A Polym. Chem.* **2011**, 49 (20), 4468–4475.
- (25) Stenström, P.; Andrén, O. C. J.; Malkoch, M. *Molecules* **2016**, 21 (3), 366.
- (26) Ghirardello, M.; Öberg, K.; Staderini, S.; Renaudet, O.; Berthet, N.; Dumy, P.; Hed, Y.; Marra, A.; Malkoch, M.; Dondoni, A. *J. Polym. Sci. Part A Polym. Chem.* **2014**, 52 (17), 2422–2433.
- (27) Walter, M. V.; Lundberg, P.; Hult, A.; Malkoch, M. *J. Polym. Sci. Part A Polym. Chem.* **2011**, 49 (13), 2990–2995.
- (28) García-Gallego, S.; Hult, D.; Olsson, J. V.; Malkoch, M. *Angew. Chemie Int. Ed.* **2015**, 54 (8), 2416–2419.

Bis-MPA Dendritic Scaffolds

Dendrimers

Name	Generation	Surface	No. Of Surface Groups	Cat. No.
Poly(ethylene glycol) linear dendrimer	generation 5	carboxyl terminated	64	911186-500MG
	generation 4	carboxyl terminated	32	911364-500MG
Poly(ethylene glycol) linear dendrimer	generation 3	carboxyl terminated	16	911259-500MG
Bis-MPA-RAFT dendrimer	generation 1	trimethylol propane core	6	911550-250MG
Bis-MPA-NHBoc dendrimer	generation 4	-	48	901322-100MG
	generation 3	trimethylol propane core	24	901329-100MG
	generation 2	trimethylol propane core	12	901330-100MG
	generation 1	trimethylol propane core	6	901333-100MG



MERCK

subscribe today

Don't miss another
topically focused technical review.

It's **free** to sign up for a print or digital subscription of *Material Matters*™.

- Advances in cutting-edge materials
- Technical reviews on emerging technology from leading scientists
- Peer-recommended materials with application notes
- Product and service recommendations



To view the library of past issues
or to subscribe, visit

SigmaAldrich.com/mm

Dendrons

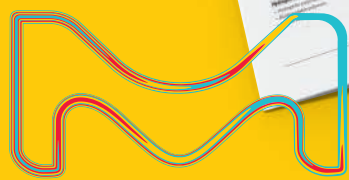
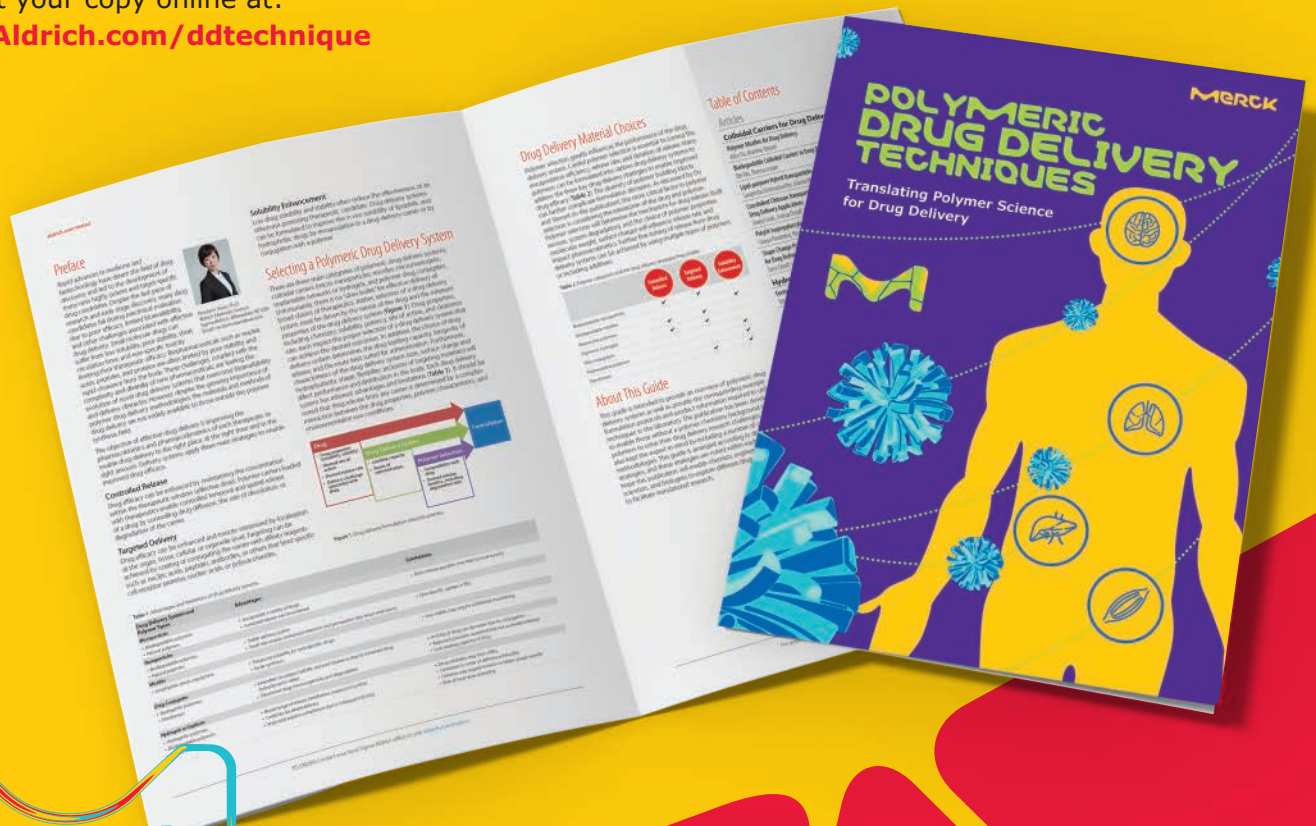
Name	Generation	Surface	No. Of Surface Groups	Cat. No.
Poly(ethylene glycol) linear dendron	4	carboxyl terminated	16	911240-250MG
	2	carboxyl terminated	4	911321-250MG
	1	carboxyl terminated	2	911313-250MG
Polyester bis-MPA dendron	3	acetylene, NHBoc (core)	8	901376-100MG
	2	acetylene, NHBoc (core)	4	901374-100MG
	1	acetylene, NHBoc (core)	2	901370-100MG
	3	carboxyl, biotin (core)	8	911291-50MG
	2	carboxyl, biotin (core)	4	911348-50MG
	1	carboxyl, biotin (core)	2	911275-50MG
	4	carboxyl, NHBoc (core)	16	901394-100MG
	3	carboxyl, NHBoc (core)	8	901398-100MG
	2	carboxyl, NHBoc (core)	4	901408-100MG
	1	carboxyl, NHBoc (core)	2	901379-100MG
	2	carboxyl, rhodamine (core)	4	911496-50MG
	4	NHBoc, acetylene (core)	16	901313-100MG
	2	NHBoc, acetylene (core)	4	901316-100MG
	4	NHBoc, azide (core)	16	901298-100MG
	3	NHBoc, azide (core)	8	901332-100MG
	2	NHBoc, azide (core)	4	901297-100MG
	1	NHBoc, azide (core)	2	901311-100MG
	3	NHBoc, biotin (core)	8	911437-50MG
	2	NHBoc, biotin (core)	4	911569-50MG
	1	NHBoc, biotin (core)	2	911577-50MG
	4	NHBoc, carboxyl (core)	16	901381-100MG
	3	NHBoc, carboxyl (core)	8	901380-100MG
	2	NHBoc, carboxyl (core)	4	901377-100MG
	1	NHBoc, carboxyl (core)	2	901393-100MG
	3	NHBoc, NHS (core)	8	911518-50MG
	2	NHBoc, NHS (core)	4	911488-50MG
	1	NHBoc, NHS (core)	2	911461-50MG
	4	NHBoc, thiol (core)	16	901304-100MG
	3	NHBoc, thiol (core)	8	901303-100MG
	2	NHBoc, thiol (core)	4	901312-100MG
	1	NHBoc, thiol (core)	2	901300-100MG
	2	rhodamine, carboxyl (core)	4	911445-50MG

IMPROVE DELIVERY

A Step-by-Step Guide

Low drug solubility and stability often reduce the effectiveness of an otherwise promising therapeutic candidate. In this comprehensive guide, you'll discover how polymers can provide the drug delivery solutions you need for controlled release, targeting, and solubility enhancement.

Request your copy online at:
SigmaAldrich.com/ddtechnique



The life science business of Merck operates as MilliporeSigma in the U.S. and Canada.

Sigma-Aldrich®
 Lab & Production Materials



Polymers with possibilities

Functionalized Poly(ethylene glycol)s for Drug Delivery

Polymer of choice for optimal and reproducible results.

When it comes to drug delivery technologies and solutions, poly(ethylene glycol)s or PEGs are the polymer of choice for optimal and reproducible results. With excellent pharmacokinetic properties, they are ideal materials for bioconjugation, pegylation, crosslinking, and hydrogel formation.

Let us help you transform your work into new therapeutic discoveries with our diverse PEG selection.

For a complete list of available materials, visit:
[SigmaAldrich.com/PEG](https://www.sigmaaldrich.com/PEG)



© 2020 Merck KGaA, Darmstadt, Germany and/or its affiliates. All Rights Reserved. Merck, Material Matters, the vibrant M, and Sigma-Aldrich are trademarks of Merck KGaA, Darmstadt, Germany or its affiliates. All other trademarks are the property of their respective owners. Detailed information on trademarks is available via publicly accessible resources.
Lit. No. MK_BR6492EN 2020-32544, 2020-32582 10/2020

The life science business of Merck operates as MilliporeSigma in the U.S. and Canada.

Sigma-Aldrich[®]
Lab & Production Materials